EUROPEAN ORGANIZATION FOR NUCLEAR RESEARCH

CERN–EP/99–144

12 October 1999

Measurement of the Gluon Fragmentation Function and a Comparison of the Scaling Violation in Gluon and Quark Jets

DELPHI Collaboration

Abstract

The fragmentation functions of quarks and gluons are measured in various three-jet topologies in Z decays from the full data set collected with the DELPHI detector at the Z resonance between 1992 and 1995. The results at different values of transverse momentum-like scales are compared. A parameterization of the quark and gluon fragmentation functions at a fixed reference scale is given. The quark and gluon fragmentation functions show the predicted pattern of scaling violations. The scaling violation for quark jets as a function of a transverse momentum-like scale is in a good agreement with that observed in lower energy e^+e^- annihilation experiments. For gluon jets it appears to be significantly stronger.
The scale dependences of the gluon and quark fragmentation functions agree with the prediction of the DGLAP evolution equations from which the colour factor ratio C_A/C_F is measured to be:

$$\frac{C_A}{C_F} = 2.26 \pm 0.09_{stat.} \pm 0.06_{sys.} \pm 0.12_{clus.,scale} \, .$$

(Submitted to Eur. Phys. J. C)

P.Abreu[22], W.Adam[52], T.Adye[38], P.Adzic[12], Z.Albrecht[18], T.Alderweireld[2], G.D.Alekseev[17], R.Alemany[51], T.Allmendinger[18], P.P.Allport[23], S.Almehed[25], U.Amaldi[9], N.Amapane[47], S.Amato[49], E.G.Anassontzis[3], P.Andersson[46], A.Andreazza[9], S.Andringa[22], P.Antilogus[26], W-D.Apel[18], Y.Arnoud[9], B.Åsman[46], J-E.Augustin[26], A.Augustinus[9], P.Baillon[9], P.Bambade[20], F.Barao[22], G.Barbiellini[48], R.Barbier[26], D.Y.Bardin[17], G.Barker[18], A.Baroncelli[40], M.Battaglia[16], M.Baubillier[24], K-H.Becks[54], M.Begalli[6], A.Behrmann[54], P.Beilliere[8], Yu.Belokopytov[9], K.Belous[44], N.C.Benekos[33], A.C.Benvenuti[5], C.Berat[15], M.Berggren[26], D.Bertini[26], D.Bertrand[2], M.Besancon[41], M.Bigi[47], M.S.Bilenky[17], M-A.Bizouard[20], D.Bloch[10], H.M.Blom[32], M.Bonesini[29], W.Bonivento[28], M.Boonekamp[41], P.S.L.Booth[23], A.W.Borgland[4], G.Borisov[20], C.Bosio[43], O.Botner[50], E.Boudinov[32], B.Bouquet[20], C.Bourdarios[20], T.J.V.Bowcock[23], I.Boyko[17], I.Bozovic[12], M.Bozzo[14], M.Bracko[45], P.Branchini[40], R.A.Brenner[50], P.Bruckman[9], J-M.Brunet[8], L.Bugge[34], T.Buran[34], B.Buschbeck[52], P.Buschmann[54], S.Cabrera[51], M.Caccia[28], M.Calvi[29], T.Camporesi[9], V.Canale[39], F.Carena[9], L.Carroll[23], C.Caso[14], M.V.Castillo Gimenez[51], A.Cattai[9], F.R.Cavallo[5], V.Chabaud[9], M.Chapkin[44], Ph.Charpentier[9], L.Chaussard[26], P.Checchia[37], G.A.Chelkov[17], R.Chierici[47], P.Chliapnikov[9,44], P.Chochula[7], V.Chorowicz[26], J.Chudoba[31], K.Cieslik[19], P.Collins[9], R.Contri[14], E.Cortina[51], G.Cosme[20], F.Cossutti[9], H.B.Crawley[1], D.Crennell[38], S.Crepe[15], G.Crosetti[14], J.Cuevas Maestro[35], S.Czellar[16], M.Davenport[9], W.Da Silva[24], G.Della Ricca[48], P.Delpierre[27], N.Demaria[9], A.De Angelis[48], W.De Boer[18], C.De Clercq[2], B.De Lotto[48], A.De Min[37], L.De Paula[49], H.Dijkstra[9], L.Di Ciaccio[9,39], J.Dolbeau[8], K.Doroba[53], M.Dracos[10], J.Drees[54], M.Dris[33], A.Duperrin[26], J-D.Durand[9], G.Eigen[4], T.Ekelof[50], G.Ekspong[46], M.Ellert[50], M.Elsing[9], J-P.Engel[10], M.Espirito Santo[22], G.Fanourakis[12], D.Fassouliotis[12], J.Fayot[24], M.Feindt[18], P.Ferrari[28], A.Ferrer[51], E.Ferrer-Ribas[20], F.Ferro[14], S.Fichet[24], A.Firestone[1], U.Flagmeyer[54], H.Foeth[9], E.Fokitis[33], F.Fontanelli[14], B.Franek[38], A.G.Frodesen[4], R.Fruhwirth[52], F.Fulda-Quenzer[20], J.Fuster[51], A.Galloni[23], D.Gamba[47], S.Gamblin[20], M.Gandelman[49], C.Garcia[51], C.Gaspar[9], M.Gaspar[49], U.Gasparini[37], Ph.Gavillet[9], E.N.Gazis[33], D.Gele[10], N.Ghodbane[26], I.Gil[51], F.Glege[54], R.Gokieli[9,53], B.Golob[9,45], G.Gomez-Ceballos[42], P.Goncalves[22], I.Gonzalez Caballero[42], G.Gopal[38], L.Gorn[1], Yu.Gouz[44], V.Gracco[14], J.Grahl[1], E.Graziani[40], P.Gris[41], G.Grosdidier[20], K.Grzelak[53], J.Guy[38], F.Hahn[9], S.Hahn[54], S.Haider[9], A.Hallgren[50], K.Hamacher[54], J.Hansen[34], F.J.Harris[36], V.Hedberg[9,25], S.Heising[18], J.J.Hernandez[51], P.Herquet[2], H.Herr[9], T.L.Hessing[36], J.-M.Heuser[54], E.Higon[51], S-O.Holmgren[46], P.J.Holt[36], S.Hoorelbeke[2], M.Houlden[23], J.Hrubec[52], M.Huber[18], K.Huet[2], G.J.Hughes[23], K.Hultqvist[9,46], J.N.Jackson[23], R.Jacobsson[9], P.Jalocha[19], R.Janik[7], Ch.Jarlskog[25], G.Jarlskog[25], P.Jarry[41], B.Jean-Marie[20], D.Jeans[36], E.K.Johansson[46], P.Jonsson[26], C.Joram[9], P.Juillot[10], L.Jungermann[18], F.Kapusta[24], K.Karafasoulis[12], S.Katsanevas[26], E.C.Katsoufis[33], R.Keranen[18], G.Kernel[45], B.P.Kersevan[45], B.A.Khomenko[17], N.N.Khovanski[17], A.Kiiskinen[16], B.King[23], A.Kinvig[23], N.J.Kjaer[9], O.Klapp[54], H.Klein[9], P.Kluit[32], P.Kokkinias[12], V.Kostioukhine[44], C.Kourkoumelis[3], O.Kouznetsov[41], M.Krammer[52], E.Kriznic[45], Z.Krumstein[17], P.Kubinec[7], J.Kurowska[53], K.Kurvinen[16], J.W.Lamsa[1], D.W.Lane[1], P.Langefeld[54], V.Lapin[44], J-P.Laugier[41], R.Lauhakangas[16], G.Leder[52], F.Ledroit[15], V.Lefebure[2], L.Leinonen[46], A.Leisos[12], R.Leitner[31], J.Lemonne[2], G.Lenzen[54], V.Lepeltier[20], T.Lesiak[19], M.Lethuillier[41], J.Libby[36], W.Liebig[54], D.Liko[9], A.Lipniacka[9,46], I.Lippi[37], B.Loerstad[25], J.G.Loken[36], J.H.Lopes[49], J.M.Lopez[42], R.Lopez-Fernandez[15], D.Loukas[12], P.Lutz[41], L.Lyons[36], J.MacNaughton[52], J.R.Mahon[6], A.Maio[22], A.Malek[54], T.G.M.Malmgren[46], S.Maltezos[33], V.Malychev[17], F.Mandl[52], J.Marco[42], R.Marco[42], B.Marechal[49], M.Margoni[37], J-C.Marin[9], C.Mariotti[9], A.Markou[12], C.Martinez-Rivero[20], F.Martinez-Vidal[51], S.Marti i Garcia[9], J.Masik[13], N.Mastroyiannopoulos[12], F.Matorras[42], C.Matteuzzi[29], G.Matthiae[39], F.Mazzucato[37], M.Mazzucato[37], M.Mc Cubbin[23], R.Mc Kay[1], R.Mc Nulty[23], G.Mc Pherson[23], C.Meroni[28], W.T.Meyer[1], E.Migliore[9], L.Mirabito[26], W.A.Mitaroff[52], U.Mjoernmark[25], T.Moa[46], M.Moch[18], R.Moeller[30], K.Moenig[9,11], M.R.Monge[14], X.Moreau[24], P.Morettini[14], G.Morton[36], U.Mueller[54], K.Muenich[54], M.Mulders[32], C.Mulet-Marquis[15], R.Muresan[25], W.J.Murray[38], B.Muryn[19], G.Myatt[36], T.Myklebust[34], F.Naraghi[15], M.Nassiakou[12], F.L.Navarria[5], S.Navas[51], K.Nawrocki[53], P.Negri[29], N.Neufeld[9], R.Nicolaidou[41], B.S.Nielsen[30], P.Niezurawski[53], M.Nikolenko[10,17], V.Nomokonov[16], A.Nygren[25], V.Obraztsov[44], A.G.Olshevski[17], A.Onofre[22], R.Orava[16], G.Orazi[10], K.Osterberg[16], A.Ouraou[41], M.Paganoni[29], S.Paiano[5], R.Pain[24], R.Paiva[22], J.Palacios[36], H.Palka[19], Th.D.Papadopoulou[9,33], K.Papageorgiou[12], L.Pape[9], C.Parkes[9], F.Parodi[14], U.Parzefall[23], A.Passeri[40], O.Passon[54], T.Pavel[25], M.Pegoraro[37], L.Peralta[22], M.Pernicka[52], A.Perrotta[5], C.Petridou[48], A.Petrolini[14], H.T.Phillips[38], F.Pierre[41], M.Pimenta[22], E.Piotto[28], T.Podobnik[45], M.E.Pol[6], G.Polok[19], P.Poropat[48], V.Pozdniakov[17], P.Privitera[39], N.Pukhaeva[17], A.Pullia[29], D.Radojicic[36], S.Ragazzi[29], H.Rahmani[33], J.Rames[13], P.N.Ratoff[21], A.L.Read[34], P.Rebecchi[9], N.G.Redaelli[28], M.Regler[52], J.Rehn[18], D.Reid[32], R.Reinhardt[54], P.B.Renton[36], L.K.Resvanis[3], F.Richard[20], J.Ridky[13], G.Rinaudo[47], I.Ripp-Baudot[10], O.Rohne[34], A.Romero[47], P.Ronchese[37], E.I.Rosenberg[1], P.Rosinsky[7], P.Roudeau[20], T.Rovelli[5], Ch.Royon[41], V.Ruhlmann-Kleider[41], A.Ruiz[42], H.Saarikko[16], Y.Sacquin[41], A.Sadovsky[17], G.Sajot[15], J.Salt[51], D.Sampsonidis[12], M.Sannino[14], Ph.Schwemling[24], B.Schwering[54], U.Schwickerath[18], F.Scuri[48], P.Seager[21], Y.Sedykh[17], A.M.Segar[36], N.Seibert[18], R.Sekulin[38], R.C.Shellard[6], M.Siebel[54], L.Simard[41], F.Simonetto[37], A.N.Sisakian[17], G.Smadja[26], O.Smirnova[25], G.R.Smith[38], A.Sokolov[44], O.Solovianov[44], A.Sopczak[18], R.Sosnowski[53], T.Spassov[22], E.Spiriti[40], S.Squarcia[14], C.Stanescu[40], S.Stanic[45], M.Stanitzki[18], K.Stevenson[36], A.Stocchi[20], J.Strauss[52], R.Strub[10], B.Stugu[4], M.Szczekowski[53], M.Szeptycka[53], T.Tabarelli[29], A.Taffard[23], F.Tegenfeldt[50], F.Terranova[29], J.Thomas[36], J.Timmermans[32], N.Tinti[5], L.G.Tkatchev[17], M.Tobin[23], S.Todorova[10], A.Tomaradze[2], B.Tome[22], A.Tonazzo[9], L.Tortora[40], P.Tortosa[51], G.Transtromer[25], D.Treille[9],

G.Tristram[8], M.Trochimczuk[53], C.Troncon[28], M-L.Turluer[41], I.A.Tyapkin[17], S.Tzamarias[12], O.Ullaland[9], V.Uvarov[44], G.Valenti[9,5], E.Vallazza[48], C.Vander Velde[2], P.Van Dam[32], W.Van den Boeck[2], W.K.Van Doninck[2], J.Van Eldik[9,32], A.Van Lysebetten[2], N.van Remortel[2], I.Van Vulpen[32], G.Vegni[28], L.Ventura[37], W.Venus[38,9], F.Verbeure[2], M.Verlato[37], L.S.Vertogradov[17], V.Verzi[39], D.Vilanova[41], L.Vitale[48], E.Vlasov[44], A.S.Vodopyanov[17], G.Voulgaris[3], V.Vrba[13], H.Wahlen[54], C.Walck[46], A.J.Washbrook[23], C.Weiser[9], D.Wicke[54], J.H.Wickens[2], G.R.Wilkinson[36], M.Winter[10], M.Witek[19], G.Wolf[9], J.Yi[1], O.Yushchenko[44], A.Zaitsev[44], A.Zalewska[19], P.Zalewski[53], D.Zavrtanik[45], E.Zevgolatakos[12], N.I.Zimin[17,25], A.Zintchenko[17], Ph.Zoller[10], G.C.Zucchelli[46], G.Zumerle[37]

[1] Department of Physics and Astronomy, Iowa State University, Ames IA 50011-3160, USA
[2] Physics Department, Univ. Instelling Antwerpen, Universiteitsplein 1, B-2610 Antwerpen, Belgium
and IIHE, ULB-VUB, Pleinlaan 2, B-1050 Brussels, Belgium
and Faculté des Sciences, Univ. de l'Etat Mons, Av. Maistriau 19, B-7000 Mons, Belgium
[3] Physics Laboratory, University of Athens, Solonos Str. 104, GR-10680 Athens, Greece
[4] Department of Physics, University of Bergen, Allégaten 55, NO-5007 Bergen, Norway
[5] Dipartimento di Fisica, Università di Bologna and INFN, Via Irnerio 46, IT-40126 Bologna, Italy
[6] Centro Brasileiro de Pesquisas Físicas, rua Xavier Sigaud 150, BR-22290 Rio de Janeiro, Brazil
and Depto. de Física, Pont. Univ. Católica, C.P. 38071 BR-22453 Rio de Janeiro, Brazil
and Inst. de Física, Univ. Estadual do Rio de Janeiro, rua São Francisco Xavier 524, Rio de Janeiro, Brazil
[7] Comenius University, Faculty of Mathematics and Physics, Mlynska Dolina, SK-84215 Bratislava, Slovakia
[8] Collège de France, Lab. de Physique Corpusculaire, IN2P3-CNRS, FR-75231 Paris Cedex 05, France
[9] CERN, CH-1211 Geneva 23, Switzerland
[10] Institut de Recherches Subatomiques, IN2P3 - CNRS/ULP - BP20, FR-67037 Strasbourg Cedex, France
[11] Now at DESY-Zeuthen, Platanenallee 6, D-15735 Zeuthen, Germany
[12] Institute of Nuclear Physics, N.C.S.R. Demokritos, P.O. Box 60228, GR-15310 Athens, Greece
[13] FZU, Inst. of Phys. of the C.A.S. High Energy Physics Division, Na Slovance 2, CZ-180 40, Praha 8, Czech Republic
[14] Dipartimento di Fisica, Università di Genova and INFN, Via Dodecaneso 33, IT-16146 Genova, Italy
[15] Institut des Sciences Nucléaires, IN2P3-CNRS, Université de Grenoble 1, FR-38026 Grenoble Cedex, France
[16] Helsinki Institute of Physics, HIP, P.O. Box 9, FI-00014 Helsinki, Finland
[17] Joint Institute for Nuclear Research, Dubna, Head Post Office, P.O. Box 79, RU-101 000 Moscow, Russian Federation
[18] Institut für Experimentelle Kernphysik, Universität Karlsruhe, Postfach 6980, DE-76128 Karlsruhe, Germany
[19] Institute of Nuclear Physics and University of Mining and Metalurgy, Ul. Kawiory 26a, PL-30055 Krakow, Poland
[20] Université de Paris-Sud, Lab. de l'Accélérateur Linéaire, IN2P3-CNRS, Bât. 200, FR-91405 Orsay Cedex, France
[21] School of Physics and Chemistry, University of Lancaster, Lancaster LA1 4YB, UK
[22] LIP, IST, FCUL - Av. Elias Garcia, 14-1°, PT-1000 Lisboa Codex, Portugal
[23] Department of Physics, University of Liverpool, P.O. Box 147, Liverpool L69 3BX, UK
[24] LPNHE, IN2P3-CNRS, Univ. Paris VI et VII, Tour 33 (RdC), 4 place Jussieu, FR-75252 Paris Cedex 05, France
[25] Department of Physics, University of Lund, Sölvegatan 14, SE-223 63 Lund, Sweden
[26] Université Claude Bernard de Lyon, IPNL, IN2P3-CNRS, FR-69622 Villeurbanne Cedex, France
[27] Univ. d'Aix - Marseille II - CPP, IN2P3-CNRS, FR-13288 Marseille Cedex 09, France
[28] Dipartimento di Fisica, Università di Milano and INFN, Via Celoria 16, IT-20133 Milan, Italy
[29] Università degli Studi di Milano - Bicocca, Via Emanuelli 15, IT-20126 Milan, Italy
[30] Niels Bohr Institute, Blegdamsvej 17, DK-2100 Copenhagen Ø, Denmark
[31] IPNP of MFF, Charles Univ., Areal MFF, V Holesovickach 2, CZ-180 00, Praha 8, Czech Republic
[32] NIKHEF, Postbus 41882, NL-1009 DB Amsterdam, The Netherlands
[33] National Technical University, Physics Department, Zografou Campus, GR-15773 Athens, Greece
[34] Physics Department, University of Oslo, Blindern, NO-1000 Oslo 3, Norway
[35] Dpto. Fisica, Univ. Oviedo, Avda. Calvo Sotelo s/n, ES-33007 Oviedo, Spain
[36] Department of Physics, University of Oxford, Keble Road, Oxford OX1 3RH, UK
[37] Dipartimento di Fisica, Università di Padova and INFN, Via Marzolo 8, IT-35131 Padua, Italy
[38] Rutherford Appleton Laboratory, Chilton, Didcot OX11 OQX, UK
[39] Dipartimento di Fisica, Università di Roma II and INFN, Tor Vergata, IT-00173 Rome, Italy
[40] Dipartimento di Fisica, Università di Roma III and INFN, Via della Vasca Navale 84, IT-00146 Rome, Italy
[41] DAPNIA/Service de Physique des Particules, CEA-Saclay, FR-91191 Gif-sur-Yvette Cedex, France
[42] Instituto de Fisica de Cantabria (CSIC-UC), Avda. los Castros s/n, ES-39006 Santander, Spain
[43] Dipartimento di Fisica, Università degli Studi di Roma La Sapienza, Piazzale Aldo Moro 2, IT-00185 Rome, Italy
[44] Inst. for High Energy Physics, Serpukov P.O. Box 35, Protvino, (Moscow Region), Russian Federation
[45] J. Stefan Institute, Jamova 39, SI-1000 Ljubljana, Slovenia and Laboratory for Astroparticle Physics,
Nova Gorica Polytechnic, Kostanjeviska 16a, SI-5000 Nova Gorica, Slovenia,
and Department of Physics, University of Ljubljana, SI-1000 Ljubljana, Slovenia
[46] Fysikum, Stockholm University, Box 6730, SE-113 85 Stockholm, Sweden
[47] Dipartimento di Fisica Sperimentale, Università di Torino and INFN, Via P. Giuria 1, IT-10125 Turin, Italy
[48] Dipartimento di Fisica, Università di Trieste and INFN, Via A. Valerio 2, IT-34127 Trieste, Italy
and Istituto di Fisica, Università di Udine, IT-33100 Udine, Italy
[49] Univ. Federal do Rio de Janeiro, C.P. 68528 Cidade Univ., Ilha do Fundão BR-21945-970 Rio de Janeiro, Brazil
[50] Department of Radiation Sciences, University of Uppsala, P.O. Box 535, SE-751 21 Uppsala, Sweden
[51] IFIC, Valencia-CSIC, and D.F.A.M.N., U. de Valencia, Avda. Dr. Moliner 50, ES-46100 Burjassot (Valencia), Spain
[52] Institut für Hochenergiephysik, Österr. Akad. d. Wissensch., Nikolsdorfergasse 18, AT-1050 Vienna, Austria
[53] Inst. Nuclear Studies and University of Warsaw, Ul. Hoza 69, PL-00681 Warsaw, Poland
[54] Fachbereich Physik, University of Wuppertal, Postfach 100 127, DE-42097 Wuppertal, Germany

1 Introduction

Collinear divergent terms appearing in perturbative QCD calculations including hadronic initial or final states can be absorbed in the definition of structure or fragmentation functions. In this way these functions, which have to be determined experimentally, become an integral part of inelastic cross-section calculations including hadrons.

Compared to the many measurements available for quark fragmentation functions [1] the information on gluon fragmentation functions is sparse. The reason is that gluons only appear as higher order contributions in the final state of e^+e^- annihilation or deep inelastic scattering. As a consequence the underlying hard scale of the measured gluon fragmentation function was so far left open. Measurements of the gluon fragmentation function at defined underlying scales and a comparison of the evolution with scale of gluon and quark fragmentation functions are the subject of this paper.

The extraction of the gluon (and quark) fragmentation function is performed from three-jet events observed in hadronic Z decays. The assignment of jets to individual gluons or quarks follows the evident analogy to tree level graphs.

As the centre-of-mass energy for all events in this analysis is equal to the Z-mass a scale dependence only becomes accessible from different three-jet topologies. The transverse momentum-like scales applied in this analysis are motivated by MLLA calculations of multihadron production (for an overview see [2,3]), in particular these scales follow from the coherence of gluon radiation.

The larger colour factor, C_A, relevant for bremsstrahlung from a gluon compared to that for a quark, C_F, causes scaling violations of the gluon fragmentation function to be stronger than that for quarks. This strong dynamical dependence of the gluon fragmentation already demands the evolution scale to be well specified. As a relatively large range of scales, similar to that covered by the PETRA experiments, is accessible in this analysis, a comparison of the scaling violation of gluon and quark jets is feasible. This is used to demonstrate the correctness of the scales employed and as an experimental cross-check of the colour factors. It is also an important check of QCD as the values of the colour factors are a direct consequence of the $SU(3)$ group structure of QCD.

This paper is organized as follows. Section 2 introduces basic definitions used throughout this paper and discusses the evolution scales and other theoretical preliminaries. Section 3 gives a brief survey of the detector, the experimental data set, event and jet selections, procedures and corrections applied to extract the gluon and (light) quark fragmentation functions. Results on the gluon and quark fragmentation functions are presented in section 4.1. Section 4.2 is devoted to the comparison of the extracted quark fragmentation functions to those measured in e^+e^- annihilation at lower energies and to gluon fragmentation functions obtained from symmetric and non-symmetric three-jet topologies. The chosen scales are validated from these comparisons and from the behaviour of the jet broadening. In section 4.3 the gluon and quark fragmentation functions are fit with a DGLAP[1] evoluted ansatz [4] for the fragmentation functions. Parameterizations of the gluon fragmentation functions are given and scaling violation for gluon and quark jets are compared in detail. A summary and conclusion are given in section 5.

[1] **D**okshitzer, **G**ribov, **L**ipatov, **A**ltarelli, and **P**arisi

2 Theory

2.1 Jet Scales

The assessment of scaling violations demands the specification of the scale underlying the process under study. This scale enters in the strong coupling and particularly specifies the size of the available phase space. It is necessarily proportional to an external scale like the centre-of-mass energy. As in the measurement of scaling violations the scale enters logarithmically, i.e. only the relative change of scale matters (see Equation 2 and 3), the external scale may be directly taken as the scale. For this analysis the situation is different. The fragmentation functions are studied for individual gluon and quark jets in three-jet events originating from Z decays. In these events the centre-of-mass energy is constant. Therefore the relevant scales for the individual jets need to be determined from the jet energies and the event topology.

The event topology is especially important since, due to the quantum nature of QCD, the soft radiation off the individual high energy partons interferes. As a consequence the radiation attributed to a hard parton is limited to opening angles determined by the angles between the hard partons. This phenomenon is called angular ordering [5]. It may be viewed as an effective reduction of the phase space available to soft radiation and thus can be absorbed in an appropriate definition of the scale. Therefore the scale relevant to this analysis will be a product of jet energy (or momentum) and angle of the hard parton, i.e. the scale will be transverse momentum-like.

Studies of hadron production in processes with non-trivial topology [6] have shown that the characteristics of the parton cascade depend mainly on the scale $\kappa = 2E_{jet}\sin\theta/2 \sim E_{jet}\theta$ where E_{jet} is the calculated jet energy and θ the angle with respect to the closest jet. For large angles ($\theta \to \pi$), this scale coincides with the centre-of-mass energy E_{CM}. κ is proportional to $\sqrt{y}$ as defined with the Durham jet finder.

Instead of using this scale definition, we chose for convenience to take the so called hardness scale

$$\kappa_H = E_{jet}\sin\frac{\theta}{2}\,,$$

as it corresponds more closely to a single jet scale, like e.g. the jet energy, which has often been taken as an intuitive scale [7,8]. This definition leaves the relative change of the scale unaltered.

A calculation of the hadron multiplicity of three-jet events [2] predicts the scale of a gluon jet, $\tilde{p}_1^T$, to be:

$$\tilde{p}_1^T = \sqrt{2\frac{(p_q \cdot p_g)(p_{\bar{q}} \cdot p_g)}{p_q \cdot p_{\bar{q}}}}\,. \tag{1}$$

For symmetric three-jet topologies the definition of $p_1^T = 1/2 \cdot \tilde{p}_1^T$ and κ_H coincide. The relative differences between these scales turn out to be below 10% for the events accepted in this analysis. As particle production from soft gluon radiation is the complementary process to scaling violations, p_1^T was also applied as the scale for gluon jets. For further comparison also the transverse momentum with respect to the leading jet $\kappa_T = E_{jet}\sin\vartheta$, where ϑ is the smaller of the two angles with respect to the axis of the most energetic jet, and E_{jet} were also tried.

Figure 1 shows the different behaviour of the scales for symmetric three-jet event topologies and Figure 2 compares the distribution of the jet energy E_{jet} and hardness κ_H for the jets of five symmetric event topologies.

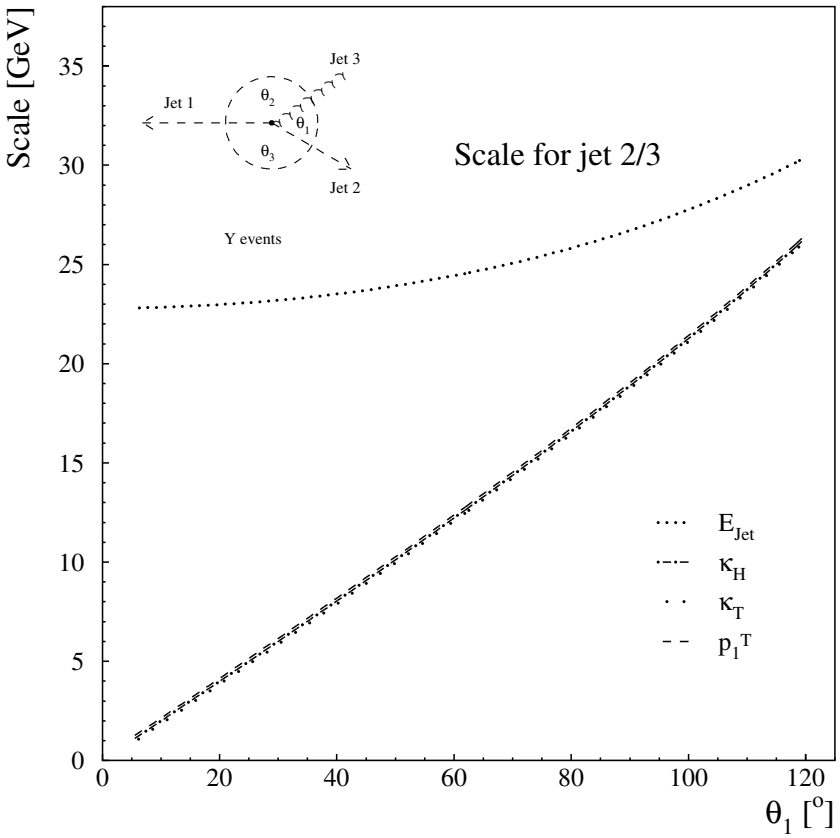

Figure 1: Different jet scales for symmetric event topologies. (For the exact definition of Y events see Section 3.4.)

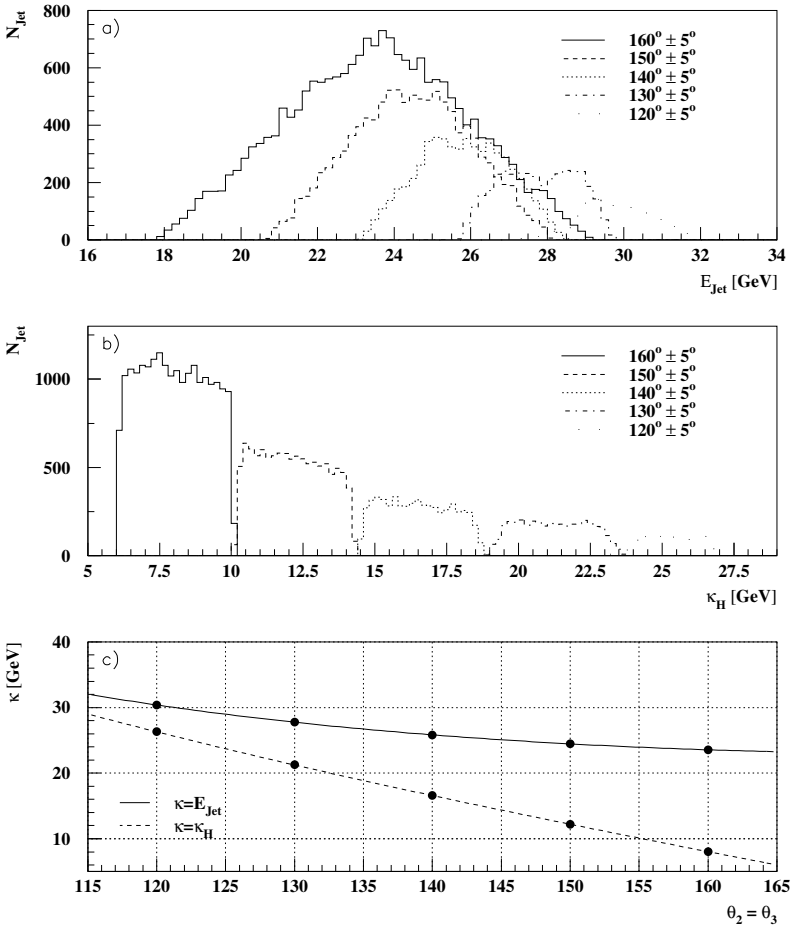

Figure 2: Separation of symmetric three-jet event topologies by the jet energy and hardness scales.

Figure 2a shows a big overlap among the energy distributions for fixed topologies. The κ_H distributions in Figure 2b are clearly separated for the different symmetric event topologies. This is understandable: in the case of symmetric events and massless jets, κ_H falls steeply to 0 with increasing $\theta_2 (= \theta_3)$, while the energy becomes nearly constant (see Figure 2c). This makes κ_H less sensitive to small deviations from the exact symmetric topology than the jet energy itself. Finally it should be noted that the relative change of scales is bigger in case of κ_H compared to E_{jet}.

2.2 Scale Dependence of the Fragmentation Function of Quark and Gluon Jets

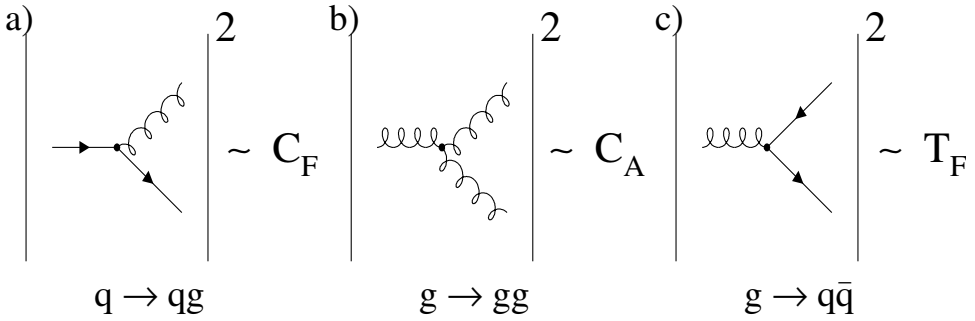

Figure 3: Diagrams of the fundamental QCD couplings

The fundamental QCD couplings are illustrated in Figure 3. The Casimir or colour factors C_F, C_A and T_F determine the apparent coupling strengths of gluon radiation from quarks (Figure 3a), of the triple-gluon vertex (Figure 3b), and of gluon splitting into a quark-antiquark pair (Figure 3c), respectively. Within $SU(3)$, these factors are $C_F = 4/3$, $C_A = 3$, and $T_F = 1/2$, which has to be weighted by the number of active quark flavors n_F (here n_F is taken to be 5).

The scale dependence (scaling violation) of gluon and quark fragmentation functions $D^H_{g,q}(x_E, s)$ into a hadron H as described by the DGLAP Equations [4] 2 and 3, is sensitive to the individual splittings depicted in Figure 3. s is the relevant scale to be replaced by the scale $(2\kappa)^2$. The complete (leading order) evolution equations for quarks and gluons are:

$$\frac{dD^H_g(x_E,s)}{d\ln s} = \frac{\alpha_s(s)}{2\pi}\cdot\int_{x_E}^1 \frac{dz}{z}\left[P_{g\to gg}(z)\cdot D^H_g(\frac{x_E}{z},s) + P_{g\to q\bar{q}}(z)\cdot D^H_q(\frac{x_E}{z},s)\right] \quad (2)$$

$$\frac{dD^H_q(x_E,s)}{d\ln s} = \frac{\alpha_s(s)}{2\pi}\cdot\int_{x_E}^1 \frac{dz}{z}\left[P_{q\to qg}(z)\cdot D^H_q(\frac{x_E}{z},s) + P_{q\to gq}(z)\cdot D^H_g(\frac{x_E}{z},s)\right]. \quad (3)$$

These equations are the transpose of the DGLAP equations for structure functions, however, this simple relation does not persist at the next-to-leading order [9]. The relevant Altarelli Parisi splitting kernels are:

$$P_{q\to qg}(z) = C_F\cdot\frac{1+z^2}{(1-z)_+} + \frac{4}{3}\cdot\frac{3}{2}\delta(1-z) \quad (4)$$

$$P_{g\to gg}(z) = 2C_A \cdot \left[z(1-z) + \frac{z}{(1-z)_+} + \frac{1-z}{z} \right] + \left(\frac{11N_C - 4n_F T_F}{6} \right) \delta(1-z) \quad (5)$$

$$P_{g\to q\bar{q}}(z) = 2n_F T_F \cdot (z^2 + (1-z)^2) \quad (6)$$

$$P_{q\to gq}(z) = C_F \cdot \frac{1+(1-z)^2}{z} \quad . \quad (7)$$

Here the 'plus' distribution $(1-z)_+$ is defined such that the integral with any sufficiently smooth distribution f is

$$\int_0^1 dx \frac{f(x)}{(1-x)_+} = \int_0^1 dx \frac{f(x)-f(1)}{1-x} \quad ,$$

$$\text{and} \qquad \frac{1}{(1-x)_+} = \frac{1}{1-x} \text{ for } 0 \le x < 1 \, .$$

The 'plus' and the δ terms stem from virtual diagrams and regularize the $1/(1-z)$ singularities. A detailed description is given in [10].

The logarithmic slope $\frac{d \ln D_p^H(x_E,s)}{d \ln s}$ for each fragmentation function independently measures the product of the strong coupling and the colour factors of the relevant splitting kernels. Thus the ratio

$$r_{\mathcal{S}}(x_E) = \frac{d \ln D_g^H(x_E,s)}{d \ln s} \Big/ \frac{d \ln D_q^H(x_E,s)}{d \ln s}$$

is, in the limit of large x_E [2], equal to the ratio of colour factors C_A/C_F. The slopes and the ratio can be predicted by solving the DGLAP equation numerically. A simultaneous fit of the gluon and quark fragmentation functions yields smaller errors for C_A/C_F than a direct measurement of $r_{\mathcal{S}}$, because the usable x_E interval can be extended. A detailed description is given in [10]. Here a program using first order splitting kernels is employed [11].

The following ansatz was used to parameterize the fragmentation functions at a fixed reference scale κ_0 to start the evolution, similar to other analyses [12,13]:

$$D_p^H(x_E) = a_3 \cdot x_E^{a_1} \cdot (1-x_E)^{a_2} \cdot \exp\left(-a_4 \cdot \ln^2 x_E\right) \quad . \quad (8)$$

The parameters $a_i^{q,g}$, Λ_{QCD} and the colour factor C_A were fitted simultaneously.

3 Data Analysis

This section describes the parts of the DELPHI detector relevant to this analysis, the particle and event selection, the jet reconstruction, the event topologies analysed, the impact parameter tagging used for selecting gluon and quark jet samples, and the subtraction method used to extract the properties of pure light quark and gluon jet samples.

3.1 The DELPHI Detector

DELPHI is a hermetic detector with a solenoidal magnetic field of 1.2 T. The tracking detectors, situated in front of the electromagnetic calorimeters are a silicon micro-vertex

[2] In the limit of large hadron energy fractions $x_E = E_{hadron}/E_{jet}$, i.e. for $x_E \ge \frac{1}{2}$, the lower energy parton in a splitting process cannot contribute. In a $q \to qg$ splitting process the lower energy parton is almost always the gluon. The $g \to q\bar{q}$ splitting is disfavoured w.r.t. $g \to gg$ (compare Equation 5-7).

detector VD, a combined jet/proportional chamber inner detector ID, a time projection chamber TPC as the major tracking device, and the streamer tube detector OD in the barrel region. The forward region is covered by the drift chamber detectors FCA and FCB.

The electromagnetic calorimeters are the high density projection chamber HPC in the barrel, and the lead-glass calorimeter FEMC in the forward region. The hadron calorimeter HAC, embedded in the iron magnetic return yoke outside the electromagnetic calorimeter and magnetic coil, provides energy and position measurements for neutral hadrons. Detailed information about the design and performance of DELPHI can be found in [14] and [15].

3.2 The Particle and Event Selection

The full data collected by DELPHI during the years 1992 to 1995 are considered in the present analysis. In a first step of the selection procedure, the quality cuts given in Tables 1 and 2 are imposed on all charged and neutral particles in order to ensure a reliable determination of their momenta and energies (ϵ is the impact parameter with respect to the primary vertex, L_{track} the measured track length;).

Variable	**Cut**	**% Loss**
p	≥ 0.3 GeV/c	19.8
θ_{polar}	$20^\circ - 160^\circ$	7.7
ϵ_{xy}	≤ 5.0 cm	4.9
ϵ_z	≤ 10.0 cm	1.1
L_{track}	≥ 30 cm	2.4
$\Delta p/p$	$\leq 100\%$	0.1

Table 1: Track selection for charged particles

Detector	E_{min} [GeV]	E_{max} [GeV]	**% Loss**
HPC	0.5	50	3.5
FEMC	0.5	30	3.4
HAC	1.0	50	10.4

Table 2: Energy cuts for neutral particles

All charged particles are assumed to be pions and all neutral particles are assumed massless. A sample of hadronic events is then selected using the cuts shown in Table 3. These demand a minimum charged multiplicity, N_{ch}, and a minimum visible energy carried by charged particles, E_{ch}^{tot}, as well as requiring the events to be well contained within the detector. E_{ch}^{hemi} denotes the sum of the energies of charged particles in the forward or backward hemisphere of the DELPHI detector. An event is discarded if the momentum of one of its charged particles is greater than p_{max}. It is additionally required that at least 5 charged particles with $p \geq 0.4$ GeV/c exist. The resulting hadronic event samples are listed in Table 5. The leptonic and two photon backgrounds are negligible, especially after selecting three-jet events for the further analysis.

Variable	**Cut**	**% Loss**
$E_{ch.}^{hemi}$	$\geq 3\%$ of $\sqrt{s}$	7.5
$E_{ch.}^{tot}$	$\geq 15\%$ of $\sqrt{s}$	0.8
$N_{ch.}$	≥ 5	0.2
$\theta_{Sphericity}$	$30^\circ - 150^\circ$	10.6
p_{max}	50% of $\sqrt{s}$	0.6

Table 3: Hadronic event selection

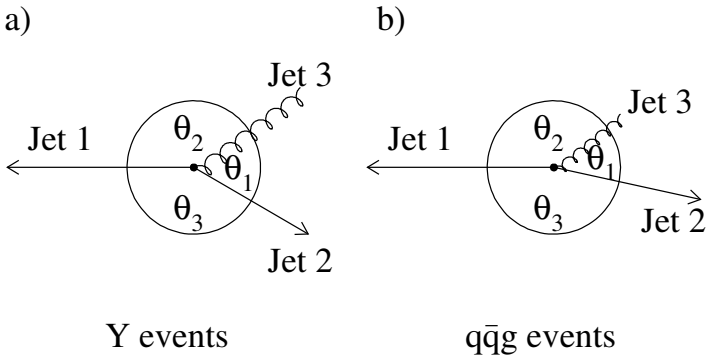

Figure 4: Event topologies of symmetric Y events and asymmetric events. θ_j are the angles between the jets after projection into the event plane.

3.3 The Jet Finding Algorithm

After the hadronic event selection, three-jet events are clustered using the Durham algorithm [16] without requiring a fixed jet resolution parameter y_{cut}. In this scheme, a jet resolution variable y_{ij} is defined for every pair of particles i and j in an event by:

$$y_{ij} = \frac{2 \cdot \min(E_i^2, E_j^2) \cdot (1 - \cos\Theta_{ij})}{E_{vis}^2} \tag{9}$$

where E_i and E_j are the energies of particles i and j, Θ_{ij} is the angle between them, and E_{vis} is the sum of all measured particle energies in the event. The corresponding particle pair with the lowest value of y_{ij} is replaced by a pseudo-particle with the sum of their four-momenta, $p_{ij} = p_i + p_j$.

The procedure is then repeated (as in [17]), re-evaluating the jet resolution variables in each iteration, until only three four-momenta are left. Each four-momentum vector remaining at the end of this process is referred to as a "jet". The properties of the jets depend both on the jet energy and the resolution scale. A fixed resolution scale would influence the jet properties, furthermore the restriction implied by a fixed jet resolution scale is rarely considered in theoretical predictions [18].

As a second algorithm the Cambridge algorithm [19] is used. It uses the same jet resolution variable y_{ij} but the particles and sub-jets are merged in inverse angular order, with the closest in angle being combined first. A freezing of soft jets is implemented to construct jets uncontaminated by coherently emitted particles (for details see [19]). Once a soft jet is resolved, it is "frozen out", i.e. it gets no extra multiplicity contribution. Here also three-jet events are clustered without using a specified y_{cut}. This corresponds to the situation proposed in [18].

3.4 Event Topologies

For a detailed comparison of quark and gluon jet properties, it is necessary to obtain samples of quark and gluon jets with nearly the same kinematics and the same scales to allow a direct comparison of the jet properties. To fulfill this condition, different event topologies were considered, as illustrated in Figure 4:

- Basic three-jet events with $\theta_2, \theta_3 \in [135° \pm 35°]$.

- Mirror symmetric events, $\theta_2, \theta_3 \in (120°, 130°, 140°, 150°, 160°) \pm 5°$, subsequently called **Y events**. These Y events are a sub-sample of the basic three-jet sample in which the two low-energy jets should be more directly comparable.

The jet axes are projected into the event plane, which is defined as the plane perpendicular to the smallest sphericity eigenvector as obtained from the quadratic momentum tensor ($M_{\alpha\beta} = \sum_{i=1}^{n} p_{i\alpha} p_{i\beta}$). The jets are numbered in decreasing order of jet energy, where the energy of each jet is calculated from the angles between the jets assuming massless kinematics:

$$E_j^{calc} = \frac{\sin\theta_j}{\sin\theta_1 + \sin\theta_2 + \sin\theta_3}\sqrt{s}, \quad j = 1, 2, 3\,, \tag{10}$$

where θ_j is the interjet angle as defined in Figure 4.

In order to enhance the contribution from events with three well-defined jets attributed to $q\bar{q}g$ production, further cuts are applied to the three-jet event samples as summarized in Table 4. These cuts select planar events with each of the reconstructed jets well contained within the sensitive part of the detector.

Measurement	Cuts	% Loss
Sum of angles between jets	$\geq 355°$	~ 0.06
Polar angle of each jet axis	$30° - 150°$	~ 12
Visible jet energy per jet	≥ 5 GeV	~ 0.11
Number of particles in each jet	≥ 2 (charged or neutral)	~ 0.38

Table 4: Planarity and acceptance selections for reconstructed jets and the % loss for the asymmetric events.

From the initial ~3,695,000 hadronic events collected by DELPHI (and ~10,507,000 Monte Carlo events), about 756,000 (2,500,000) asymmetric three-jet events remain (see Table 5, the symmetric three-jet events are fully included in this sample).

	Hadronic Events		**Asymmetric Events**	
Year	Data	Simulation	Data	Simulation
1992	604490	1723829	164450	499380
1993	608025	1605915	164609	464975
1994	1198034	4304445	271343	1246130
1995	577196	1029486	155750	297202
total	2987745	8663675	756152	2507687

Table 5: Samples of the analysed hadronic events and the selected asymmetric events.

3.5 Quark and Gluon Jet Identification

A sample rich in gluon jets is obtained from three-jet events which originate from Z decays to a $b\bar{b}$ pair. The events are identified using a well established lifetime-tag

technique, and the gluon jets are tagged indirectly by identifying the other two jets as b-quark jets.

The light (udsc) quark jets used for comparison to these gluon jets are taken from events failing the event level lifetime-tag. These jet samples, including the corresponding gluon jets, are called "normal mixture"

In practice, subtracting the small residual heavy quark contributions from the b tagged sample yields a pure gluon sample. The properties of light quark jets are obtained by subtracting the gluon distributions from the distributions measured in the normal mixture jet sample.

In this way neither the gluon nor the light quark distributions are significantly biased by the b-quark identification procedure. However the jets identified as b-quark jets are biased. More importantly, about half of the particles in b jets come from the weak decays of B-hadrons. Thus b jets cannot be used for a direct comparison with gluon jets within a purely QCD framework neglecting these decays.

In the following, the selection of the gluon and the normal mixture jet samples in asymmetric events is described in detail as well as the corrections applied to obtain information on pure quark and gluon jets.

3.5.1 Lifetime Tags at Event and Jet Level

The combined impact parameters and their error distributions are used to construct an algorithm for tagging b jets [20]. Basically, in this method, the variable, P_N, for the hypothesis that all tracks arise directly from the e^+e^- annihilation point is evaluated for a given selection of N tracks. By construction, light quark events or jets have a flat distribution in P_N while, because of the long lifetimes of B-hadrons, events or jets containing b-quarks tend to give low values.

Events with a b-quark signature are selected as input to the gluon identification by demanding that P_E, the value of P_N evaluated for the whole event, does not exceed -0.97. It is often more convenient to use the variable $\lambda_E = P_E + 2 = 1.03$. Events failing the b tag are considered to be in the normal mixture sample.

The tracks corresponding to each of the reconstructed jets are then used to construct a variable P_J per jet. Jets are finally classified according to the observed values of P_J following this strategy:

The most energetic jet is assumed to be a quark jet. Cuts on $\lambda_J = P_J + 2$ are applied to each of the two lower energy jets in order to decide which is the quark jet and which is the gluon jet. The main criterion applied is to demand that one of the two lower energy jets satisfies the condition $\lambda_J < 1.28$. The remaining jet is then taken as the gluon jet provided its value λ_J is above 1.28. This ensures that the decay products of the B-hadrons do not, in general, filter through to the selected sample of gluon jets. In total, 142,413 gluon jets in the asymmetric event sample are selected using this single jet tag method.

In Figure 5, the distribution of the jet tagging variable, λ_J, measured in Y events ($\theta_2, \theta_3 \in [150^\circ \pm 15^\circ]$) is compared separately for normal mixture jets, charm jets, b-quark jets, and gluon jets as predicted by the Monte Carlo simulations.

3.5.2 Gluon and Quark Jet Purities

Efficiency and purity calculations were made using events generated by the JETSET 7.3 Monte Carlo [21] tuned to DELPHI data [22] and passed through the full simulation

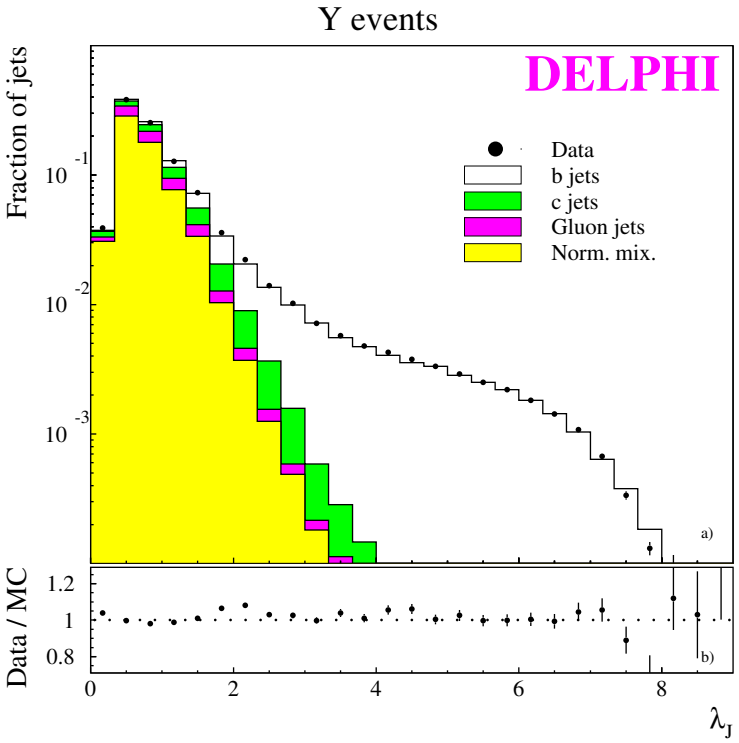

Figure 5: Jet variables as measured from the data and as predicted by the Monte Carlo for normal mixture (in *uds* events), *c*-quark, *b*-quark, and gluon jets (in *c* and *b* events) for Y events with $\theta_2, \theta_3 \in [150° \pm 15°]$.

program (DELSIM [15,23]) of the DELPHI detector and the standard DELPHI data reconstruction chain. Even in the Monte Carlo, the assignment of parton flavours to the jets is not unique, as in parton models like JETSET the history is interrupted by the building of strings. Thus two independent ways of defining the gluon jet in the fully reconstructed Monte Carlo *b* and *c* event samples were investigated [24]:

- **angle assignment:** The gluon induced jet is assumed to be the jet making the largest angle with the nearest B/D-hadron originating from the primary b/c-quarks.
- **PS assignment:** First the partons are clustered to three jets if the event is accepted as containing three well measured jets at hadron level. Quarks are given a weight of $+1$, antiquarks a weight of -1, and gluons a weight of 0. Parton jets are identified as quark and gluon jets if the sum of the flavour weights of all partons in a certain parton jet is +1, -1, and 0, respectively. The small amount (2%) of events not showing this expected pattern are discarded. A gluon jet is identified as the parton for which the sum of the parton flavours is 0. These parton jets are mapped onto the hadron jets in such a way that the sum of the angles between the three hadron jets and their corresponding parton jets is minimized.

Table 6 shows that the angle and PS assignments give similar results and that therefore the purities can be estimated with small systematic uncertainties. By using the PS assignment in Monte Carlo events, the gluon jets can be identified as well in b/c-events as in light quark events; hence this method is used rather than the hadron assignments. With the tagging procedure described in this section, gluon jet purities from 40% to 90% are achieved, depending on the jet scale (see Figure 6). Here the purity is defined as the

Method		Angle assignment		
	gluon in:	Jet 1	Jet 2	Jet 3
PS assignment	Jet 1	4.2%	0.01%	0.01%
	Jet 2	0.0%	25.5%	0.37%
	Jet 3	0.01%	0.15%	69.8%

Table 6: Correlation of angle and PS assignments. The table was obtained for arbitrary three-jet events with $\theta_2, \theta_3 \in [110°, 170°]$. These events also contain the symmetric events. A similar behaviour is observed concerning an assignment based on the history information of the Monte Carlo models [**?**].

ratio of the number of real tagged gluons (i.e. jets originating from gluons) to the total number of jets tagged as gluons.

3.5.3 Corrections

In a first step the pure generated light and c-quark, b-quark, and gluon Monte Carlo distributions are mixed to represent the flavour composition of the data.

Secondly, the effects of finite resolution and acceptance of the detector are corrected using a full simulation of the DELPHI detector. A linear correction function C,

$$C_i^{acc} = \frac{D^{gen}}{D^{MC+det}} \ ,$$

is determined. This correction function adjusts the distribution D^{MC+det} to D^{gen} for each bin i of any distribution of an observable. Here D^{gen} includes the total generated state before detector simulation and D^{MC+det} the state after detector simulation, which fulfills also the data selection criteria. All effects caused by the detector are included within this correction. Multiplying the measured data distribution D_i^{meas} by the correction function yields the acceptance corrected data distribution:

$$D_i^{corr} = C_i^{acc} \cdot D_i^{meas} \ .$$

Finally, in order to achieve pure quark ($udsc$) and gluon jet distributions the following equation was solved by matrix inversion:

$$\begin{pmatrix} D_n \\ D_b \\ D_g \end{pmatrix}_{\text{corrected}} = \begin{pmatrix} f_{nq} f_{nb} f_{ng} \\ f_{bq} f_{bb} f_{bg} \\ f_{gq} f_{gb} f_{gg} \end{pmatrix} \begin{pmatrix} D_q \\ D_b \\ D_g \end{pmatrix}_{\text{pure}} \ . \tag{11}$$

The f_{ij} denote the relative fraction of a parton j within the identified measured distribution i. Here i stands for a normal mixture (n), b-quark (b) or gluon (g) jet.

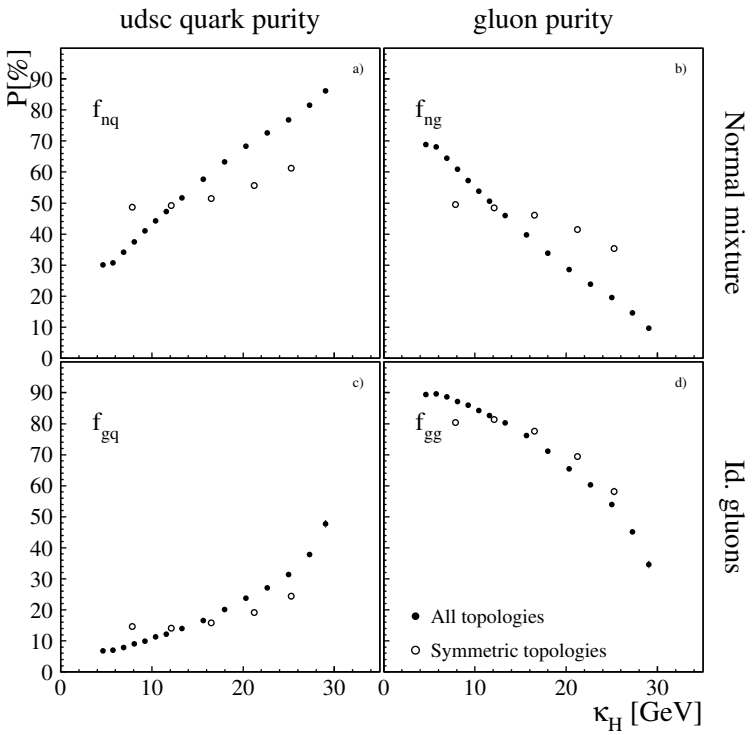

Figure 6: Gluon and quark fractions in identified gluon jets and in normal mixture jets ($f_{nq}, f_{ng}, f_{gq}, f_{gg}$). The decreasing fraction of gluon jets within normal mixture jets is due to the fact that the probability of gluon bremsstrahlung gets smaller with increasing $p_\perp$ of the gluons. Consequently a gluon fraction of $\simeq 35\%$ in the identified gluon set for high κ_H is a significant enrichment compared to the corresponding gluon fraction of $\simeq 15\%$ in the normal mixture jets.

4 Results

4.1 The General Behaviour of Gluon and Quark Fragmentation Functions

Sizeable differences were observed between the scaled energy (x_E)-distributions of stable hadrons produced in quark and gluon jets [24–26]. In Figure 7 and 8 the fragmentation functions for quark and gluon jets in the overall sample of three-jet events are shown for three different average values of κ_H. An approximately exponential decrease of the fragmentation function with increasing x_E is seen, which is stronger in the gluon case. A softening of the fragmentation functions with increasing κ_H is observed. This effect is more pronounced for gluon jets than for quark jets.

Tables of the quark fragmentation functions for different values of κ_H and the gluon fragmentation functions for different values of κ_H and p_1^T with their statistical error are available in the Durham/RAL HEP-database [27] both for the Durham and Cambridge cluster algorithms.

In order to determine systematic uncertainties of the measurements of the fragmentation functions the following sources of error were studied:

1. **Minimum number of particles per jet**
   The minimum number of particles in each jet was changed from two up to four. This has no effect for the quark jets and a $\simeq \pm 2\%$ effect is visible for the gluon jets.
2. **Minimum angle between the jets and the beam**
   The cut on the polar angle of each jet axis to the beam direction was changed from 30° to 40°. This again has no effect for the quark jets and the effect is $\leq \pm 1\%$ for the gluon jets.
3. **c depleted event sample**
   The b event tag was varied to account for a different composition (b and c depleted) of quark flavours in the normal mixture sample. No effect was observed.
4. **Variation of the parton jets assignment**
   Different quality cuts were performed to map the three parton jets to the three hadron jets. We see a $\leq \pm 2\%$ effect for quarks and a $\leq 3\%$ effect for gluons which only appears at scales < 10 GeV.

Figure 9 compares the gluon and the quark fragmentation functions for symmetric three-jet events with $\theta_2, \theta_3 \in [150° \pm 15°]$ (Durham algorithm). Quark jets fragment much harder than gluon jets. The extra suppression of the fragmentation function at high x_E (by almost one order of magnitude) measured in gluon jets relative to quark jets is expected because, contrary to the quark case, the gluon cannot be present as a valence parton inside the produced hadron. The valence quarks of the hadrons first have to be produced in a $g \to q\bar{q}$ splitting process. The softer behaviour of the gluon fragmentation function may also be due to the intrinsically larger scaling violations in gluon jets which, in combination with recoil effects (for a thorough discussion see [18]), leads to a softer hadron spectrum.

In order to demonstrate qualitatively the connection between the strength of the scaling violation at high x_E and the increase in particle multiplicity which happens predominantly at very small particle energies we compare in Figure 10 and 11 the ξ-distributions ($\xi = -\ln x_E$) which are measured for particles assigned to individual gluon (Figure 11) and quark (Figure 10) jets for different values of p_1^T and κ_H respectively . Jets here were defined using the Cambridge algorithm as this has an improved behaviour in reconstructing the gluon jets [19]. As the emission of very soft (i.e. large ξ) particles is expected to

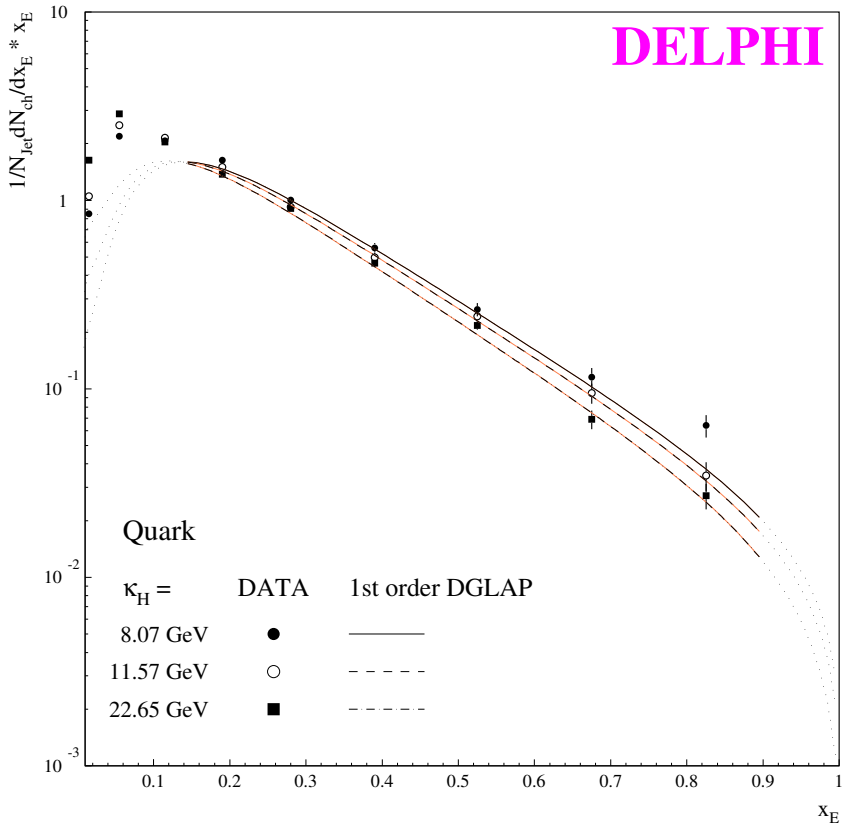

Figure 7: Scaled hadron energy distributions for quark jets for different scale values of κ_H (Durham algorithm). The 1st order DGLAP fit is superimposed. The dotted part of the lines is the extrapolation outside the fit range.

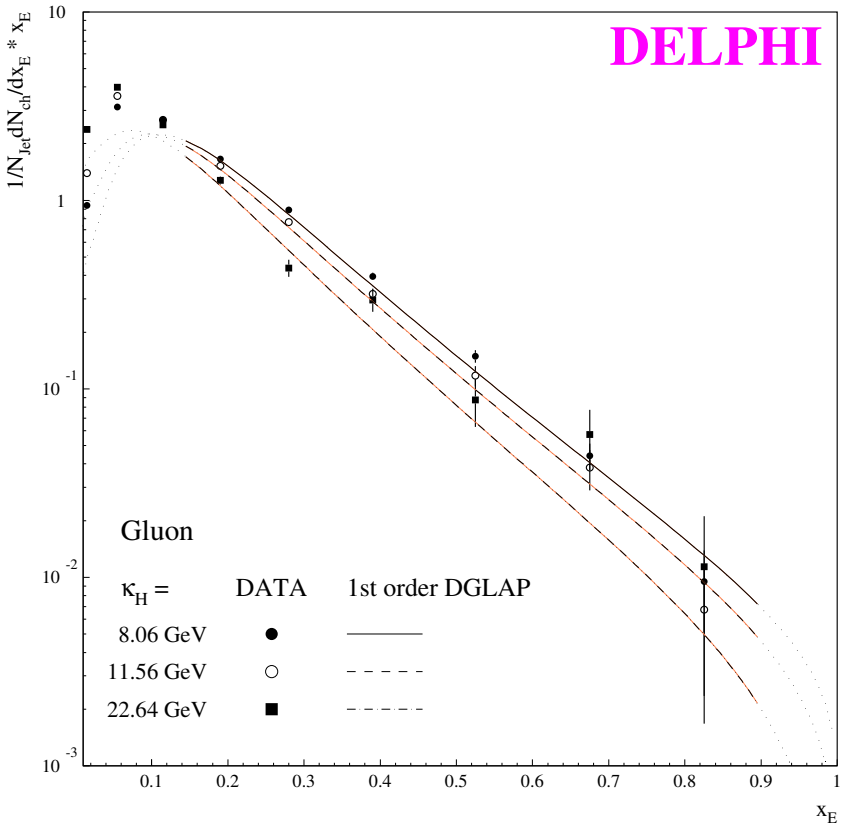

Figure 8: Scaled hadron energy distributions for gluon jets for different scale values of κ_H (Durham algorithm). The 1st order DGLAP fit is superimposed. The dotted part of the lines is the extrapolation outside the fit range.

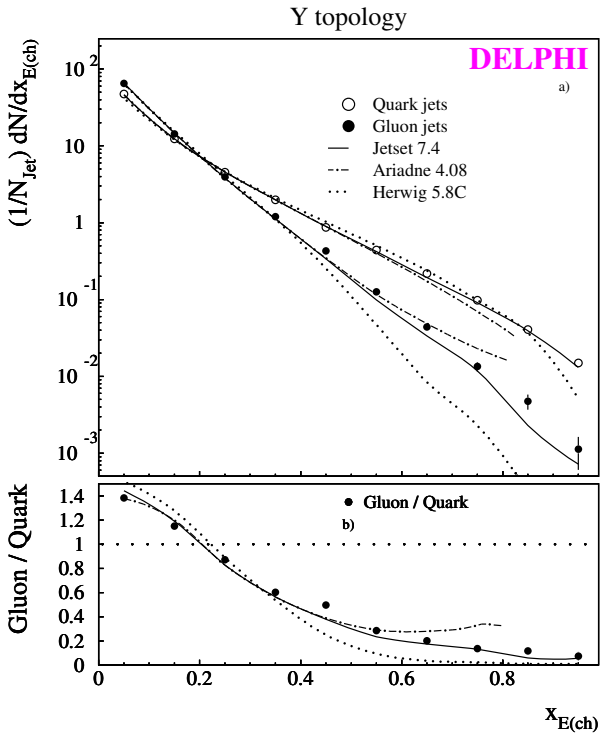

Figure 9: Gluon and the quark fragmentation functions of Y events, $\theta_2, \theta_3 \in [150° \pm 15°]$, compared to the prediction of various fragmentation models (Durham algorithm).

happen coherently from the $q\bar{q}g$ ensemble, the assignment of these particles to individual jets is to some extent arbitrary. Neglecting this complication, from the behaviour of the data in Figure 10 and 11 it is evident that scaling violation as well as the increase in multiplicity is stronger for gluon jets compared to quark jets. This is a consequence of the higher colour factor of the gluons and thus of their apparent higher "coupling" to soft gluon radiation.

The lines in Figure 10 and 11 are simple Gaussian fits to the data applied in the region of the maxima of the ξ distributions. The values of the maxima, ξ^*, of these fits together with their statistical errors are given in Table 7 and 8 (both for the Durham and Cambridge cluster algorithms). An approximately linear increase of ξ^* as a function of the scale κ_H for quarks or κ_H or p_1^T for gluons is observed, similar to the behaviour in overall e^+e^- events at different centre-of-mass energies. For gluons this increase differs significantly between κ_H and p_1^T and also between Durham and Cambridge algorithms. Due to the subtlety of assigning low energy particles to individual jets this increase should, however, not be quantitatively compared to the overall e^+e^- data.

The measurement of ξ^* for individual gluon and quark jets allows, in principle, to test a QCD prediction [28] for the difference of the peak positions for gluons and quarks:

$$\Delta\xi^* = \xi_g^* - \xi_q^* \simeq \frac{1}{12}\left(1 + \frac{n_F}{N_C^3}\right) + \mathcal{O}(\sqrt{\alpha_S}) \sim 0.1 \qquad (12)$$

at asymptotically high energies. Note that the higher order corrections in Equation 12 are expected to be sizable, moreover there may be differences due to the misassignment

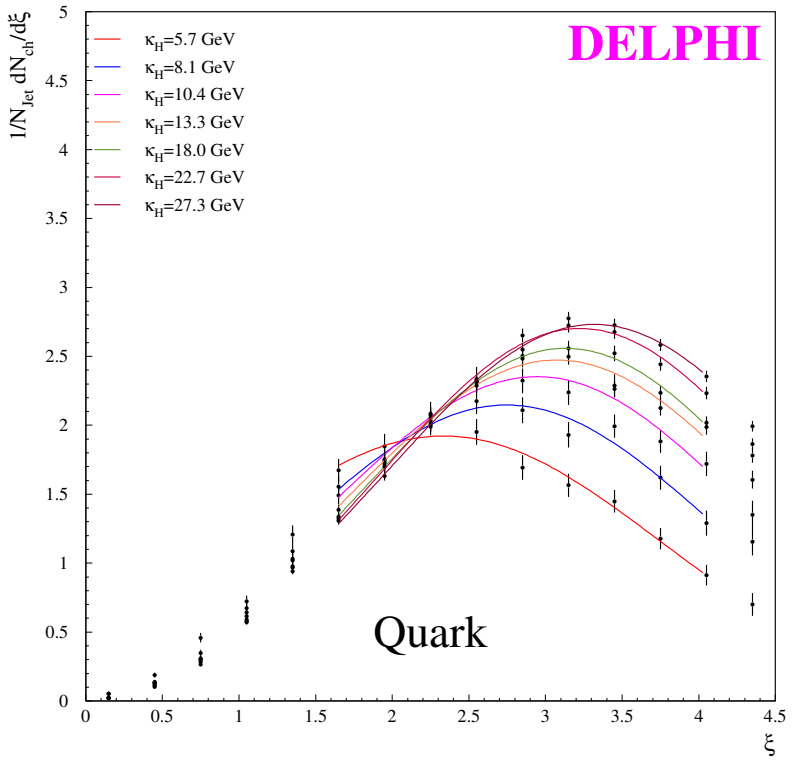

Figure 10: ξ quark distributions for different hardness scales (Cambridge algorithm). The lines are simple Gaussian fits to the data.

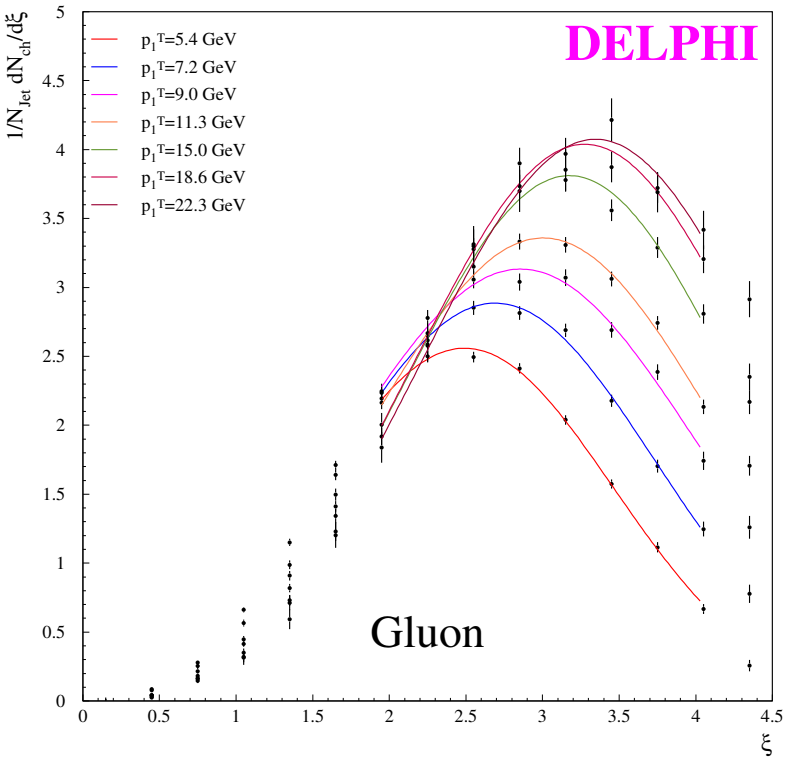

Figure 11: ξ gluon distributions for different p_1^T scales (Cambridge algorithm). The lines are simple Gaussian fits to the data.

Quark Jets				Gluon Jets							
κ_H	ξ^*	$\pm$	$\chi^2/n.d.f.$	p_1^T	ξ^*	$\pm$	$\chi^2/n.d.f.$	κ_H	ξ^*	$\pm$	$\chi^2/n.d.f.$
5.73	2.49	0.04	0.93	5.36	2.62	0.02	2.06	5.73	2.60	0.02	0.54
6.90	2.67	0.03	0.38	6.27	2.73	0.02	1.98	6.89	2.73	0.01	0.49
8.07	2.74	0.04	1.14	7.19	2.80	0.01	1.12	8.06	2.81	0.01	2.13
9.24	2.81	0.03	0.69	8.10	2.87	0.01	2.51	9.24	2.89	0.01	2.37
10.41	2.89	0.03	0.65	9.03	2.91	0.02	1.47	10.41	2.95	0.01	1.14
11.57	2.88	0.03	1.37	9.95	2.98	0.02	2.19	11.56	3.05	0.02	3.19
13.30	3.05	0.02	2.05	11.29	3.06	0.01	3.16	13.27	3.09	0.01	1.78
15.64	3.08	0.02	1.13	13.13	3.12	0.01	0.86	15.61	3.19	0.02	0.80
17.98	3.14	0.02	0.23	14.96	3.20	0.02	1.90	17.97	3.26	0.02	0.48
20.31	3.19	0.02	1.92	16.81	3.23	0.02	0.50	20.29	3.33	0.03	1.80
22.65	3.23	0.02	0.87	18.64	3.27	0.03	0.82	22.64	3.40	0.04	1.50
24.99	3.29	0.02	0.71	20.48	3.35	0.04	0.95	24.95	3.45	0.05	0.52
27.27	3.33	0.03	0.78	22.30	3.36	0.04	0.77	27.20	3.49	0.07	1.22
29.04	3.40	0.05	0.84	24.15	3.39	0.05	0.67	29.00	3.42	0.14	0.18

Table 7: ξ^* values (Durham algorithm)

of soft particles to the individual jets. At the current energies also residual shifts due to leading particle effects may be expected.

For the Durham algorithm, an about constant shift between quarks and gluons is observed which amounts to $0.10 \pm 0.01 (0.05 \pm 0.01)$ for the scale κ_H (the mixed scales p_1^T and κ_H) respectively. In case of the Cambridge algorithm, an increase from small values at low scales to $\Delta\xi^* \sim 0.15$ at large κ_H is observed. In the mixed scale (κ_H, p_1^T) case this increase of $\Delta\xi^*$ with scale is weak and $\Delta\xi^*$ is consistent with 0.

4.2 Examining Jet Scales

The mean values of the jet broadening,

$$\beta = \frac{\sum |\vec{p}_i \times \vec{r}_{jet}|}{2 \sum |\vec{p}_i|}, \tag{13}$$

are shown in Figure 12 as a function of the jet scale. The $\vec{p}_i$ are the momenta of the tracks belonging to one jet and $\vec{r}_{jet}$ is the corresponding jet direction. The β-variable is constructed analogously to the event shape observable B [29] to give a quantitative measurement of the angles of the particles w.r.t the jet axis i.e. the "broadness" of the jet. $\langle\beta\rangle$ for gluons and quarks is approximately constant for the scale κ_H. Gluon jets are observed to be wider than quark jets as expected from the different quark and gluon colour structure. The ratio of the average values of β is typically 1.5 for all scale values if κ_H is taken as the scale. Choosing instead the jet energy E_{jet} as an intuitive scale results in a strong decrease of $\langle\beta\rangle$ with increasing scale values. Alternatively the jet transverse momentum scale leads to a strong increase with increasing scale values (see lines in Figure 12).

The approximate constancy of $\langle\beta\rangle$ implies that here the longitudinal and transverse momenta scale when increasing κ_H, as would be expected for a relevant scale. This scale

Quark Jets				**Gluon Jets**							
κ_H	ξ^*	$\pm$	$\chi^2/n.d.f.$	p_1^T	ξ^*	$\pm$	$\chi^2/n.d.f.$	κ_H	ξ^*	$\pm$	$\chi^2/n.d.f.$
5.74	2.33	0.07	0.64	5.37	2.49	0.02	0.85	5.74	2.48	0.02	1.70
6.90	2.69	0.04	1.41	6.28	2.59	0.02	0.97	6.90	2.60	0.01	0.79
8.07	2.74	0.04	0.86	7.19	2.69	0.02	0.74	8.07	2.72	0.01	0.99
9.24	2.83	0.04	1.43	8.11	2.79	0.02	1.15	9.23	2.83	0.01	2.86
10.41	2.94	0.04	0.86	9.03	2.86	0.02	1.64	10.41	2.89	0.01	1.59
11.57	2.97	0.03	0.69	9.94	2.93	0.02	0.82	11.57	2.98	0.02	1.15
13.30	3.07	0.03	1.46	11.30	3.00	0.01	0.93	13.28	3.06	0.01	1.23
15.64	3.10	0.02	1.29	13.13	3.11	0.01	0.71	15.62	3.16	0.01	1.25
17.98	3.13	0.02	0.37	14.96	3.18	0.02	1.45	17.96	3.25	0.02	0.74
20.32	3.19	0.02	2.28	16.81	3.21	0.02	0.43	20.30	3.31	0.03	2.11
22.66	3.23	0.02	0.88	18.64	3.28	0.03	0.73	22.64	3.38	0.04	0.71
24.99	3.27	0.02	0.74	20.46	3.30	0.03	1.68	24.95	3.47	0.05	0.99
27.27	3.32	0.02	0.58	22.29	3.34	0.04	0.84	27.19	3.49	0.07	0.36
29.04	3.43	0.06	0.78	24.15	3.40	0.05	0.67	29.01	3.37	0.12	0.70

Table 8: ξ^* values (Cambridge algorithm)

takes phase space effects properly into account and makes jets of different topologies directly comparable. This is similarly so for the scale p_1^T (see dotted line in Figure 12). A similar scaling behaviour is observed for the event shape observable B as a function of the centre-of-mass energy $\sqrt{s}$ [30]. The observed small energy dependence in this case can be traced back to the running of α_S and to power corrections. The obviously different behaviour for E_{jet} or κ_T strongly indicates that these variables are unsuitable as choices.

Figure 13 shows the comparison of the quark fragmentation function for fixed x_E as a function of the scale κ_H with the quark fragmentation functions measured at lower energy e^+e^- experiments [1] and at high centre-of-mass energies with DELPHI. These data distributions are obtained from e^+e^- events scaled by $\frac{1}{2}$ to account for the different number of primary partons. A good agreement is seen, both in normalization and slopes. This also is an a posteriori justification of this analysis and yields a new approach to study dynamical dependencies of hadron distributions.

Figure 14 shows the gluon fragmentation functions for fixed x_E as a function of the scale κ_H. The results obtained from the overall data set and from the symmetric events agree well. This is not the case if, for instance, E_{jet} is chosen as the scale [31]. The good agreement of the three-jet quark distributions from e^+e^- data and of the symmetric gluon jets with gluon jets of any topology indicates again that $\kappa_H = E \cdot \sin\theta/2$ is a relevant scale for dynamical studies of jet properties.

The expected power behaviour, shown by a linear behaviour in the log-log plots, is fitted by:

$$D(x_E, \kappa) = a \cdot \kappa^b, \tag{14}$$

indicated by the solid lines in the Figures 13,14. The typical behaviour of scaling violations is observed in both figures, namely a strong fall off at large x_E which diminishes with falling x_E. The slope vanishes around $x_E \sim 0.1$, and finally for small x_E turns into a rise. The rise at small x_E causes the increase of multiplicity with the scale [17] (compare

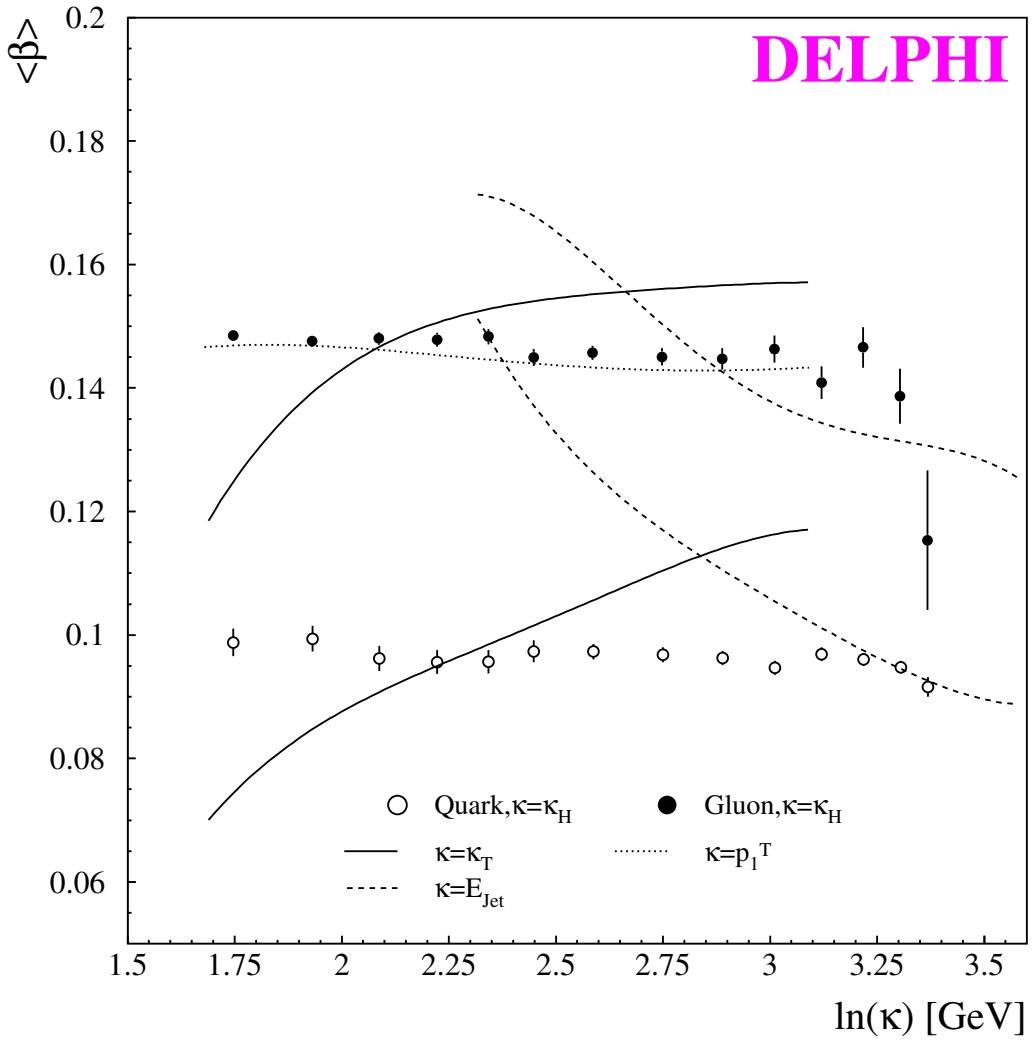

Figure 12: Mean values of the jet broadness β as a function of different jet scales (Durham algorithm). The dashed, dotted, and full curves are polynomial fits to the $\kappa = E_{jet}$, $\kappa = p_1^T$, and $\kappa = \kappa_T$ results.

also Figure 10 and 11). The scaling violation behaviour is much stronger for gluons than for quarks. This is expected due to the higher colour charge of gluons.

4.3 Scaling Violations

Figures 15 and 16 show the measured quark and gluon fragmentation distributions as a function of the scale κ_H. A fit of the fragmentation functions including a simultaneous DGLAP evolution is also shown.

For the evolution the fragmentation functions were parameterized at the reference scale $\kappa_{H,0} = 5.5$ GeV over the x_E range $0.15 \leq x_E \leq 0.9$ according to Equation 8. The parameters of the fit, for the Durham algorithm and the scale κ_H are given in Table 9. For the fit the range 6.5 GeV $\leq \kappa_{\rm H} \leq$ 28 GeV was used. To obtain a parametrization of the fragmentation functions for a broad range of the scale κ_H an ansatz similar to that

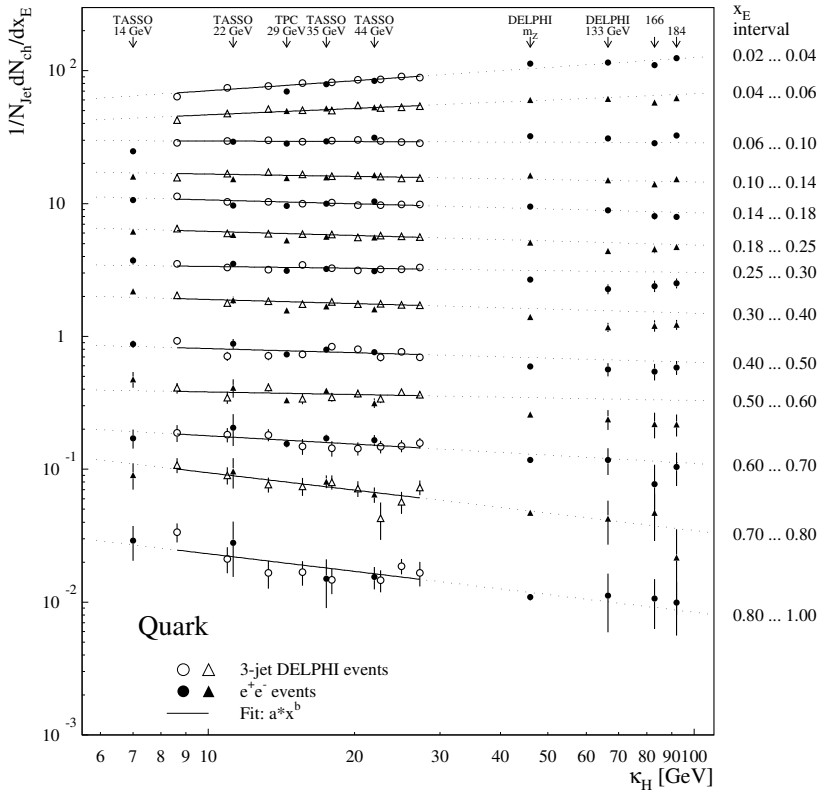

Figure 13: Scale dependence of the quark fragmentation function (Durham algorithm). The reference data stem from low and higher energy experiments. The solid line is the result of power law fits. The dotted part of the lines is the extrapolation outside the fit range.

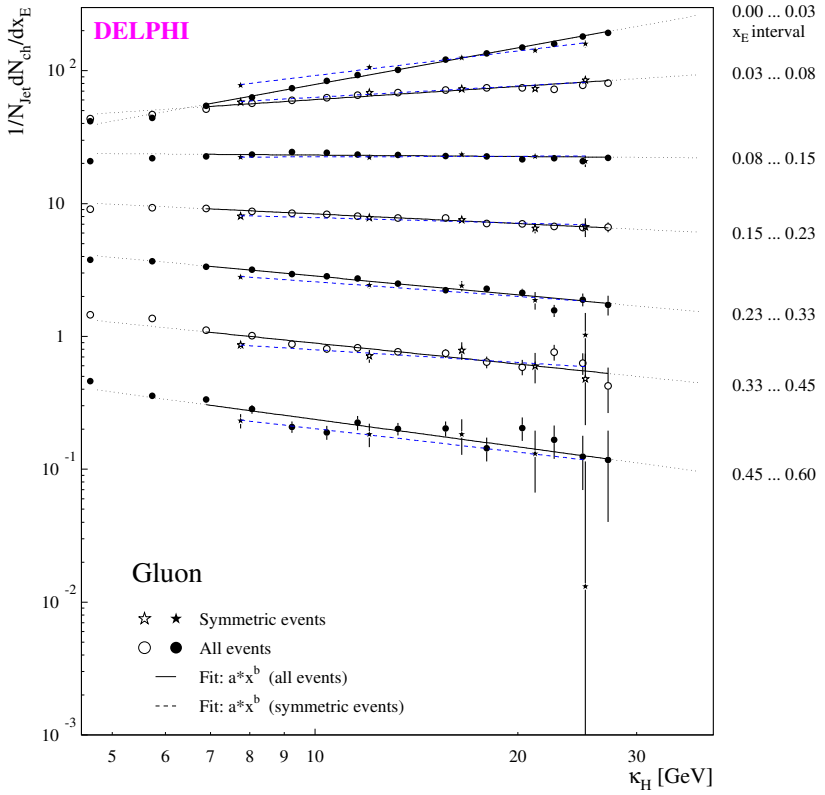

Figure 14: Scale dependence of the gluon fragmentation function (Durham algorithm). The solid (dashed) lines result from power law fits to all (to symmetric) events. The dotted part of the lines is the extrapolation outside the fit range.

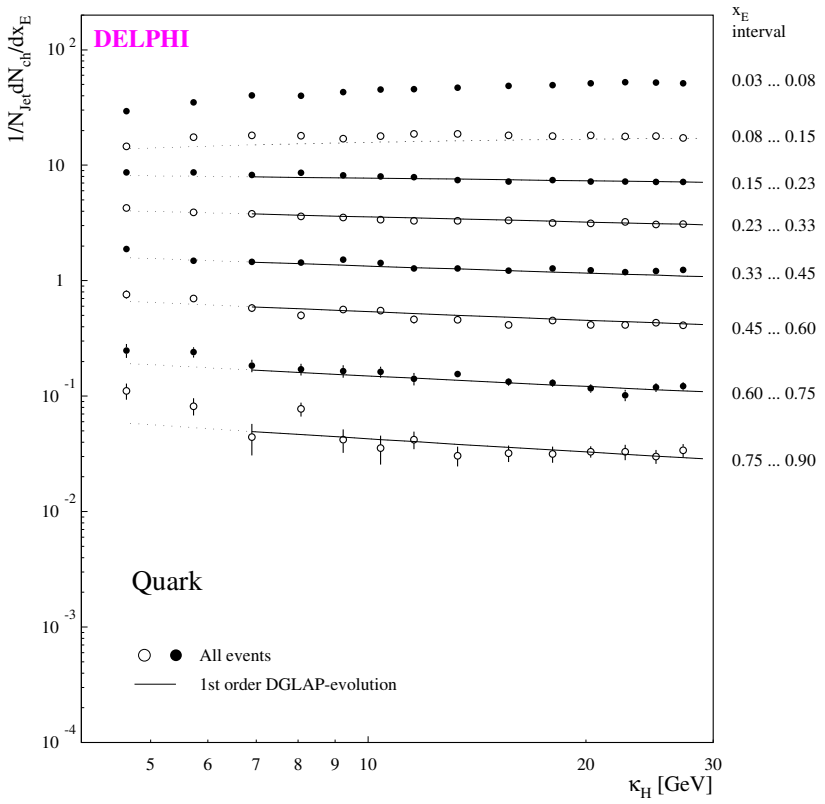

Figure 15: Scale dependence of the quark fragmentation functions (Durham algorithm). The full line is the fit of the DGLAP evolution of the fragmentation function. The dotted part of the curve is the extrapolation outside the fit range.

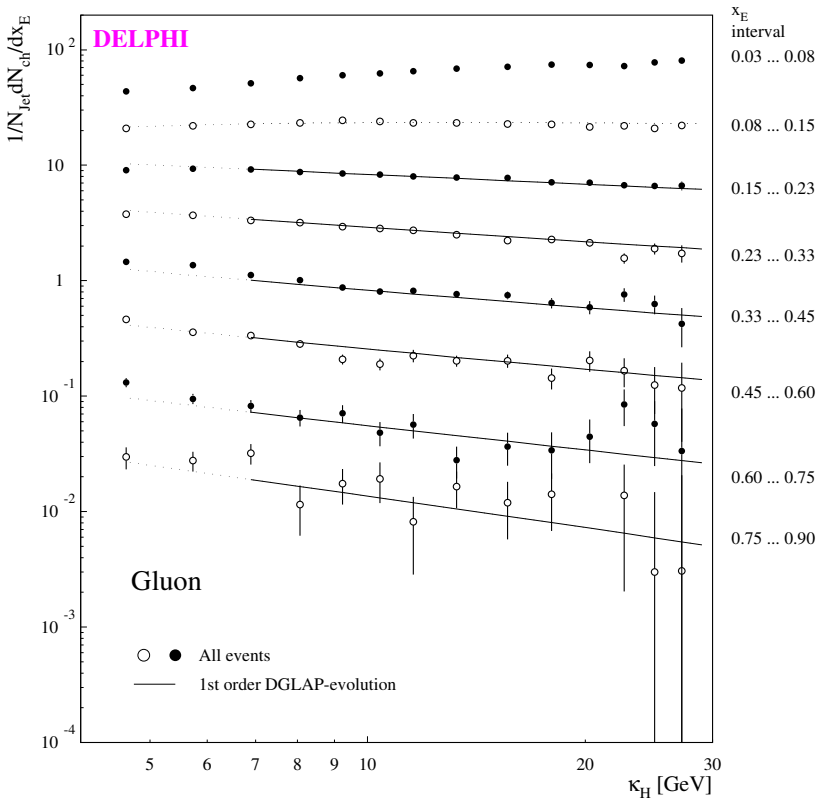

Figure 16: Scale dependence of the gluon fragmentation functions (Durham algorithm). The full line is the fit of the DGLAP evolution of the fragmentation function. The dotted part of the curve is the extrapolation outside the fit range.

	Quark Jets	**Gluon Jets**
a_1	-4.74 $\pm$ 0.22	-6.27 $\pm$ 0.32
a_2	0.58 $\pm$ 0.10	0.28 $\pm$ 0.19
a_3	0.059 $\pm$ 0.011	0.011 $\pm$ 0.003
a_4	1.024 $\pm$ 0.070	1.29 $\pm$ 0.10
$C_A = 2.97 \pm 0.12$		
$\Lambda_{\mathrm{QCD}} = (397 \pm 113)\mathrm{MeV}$		

Table 9: Parameters of the simultaneously fitted fragmentation functions at $\kappa_{H,0} = 5.5$ GeV ($\chi^2/n.d.f \sim 1.4$). The errors are given neglecting correlations between the parameters.

applied in [32] yields:

$$D(x,\kappa^2) = N_{g,q} \cdot x_{g,q}^{\alpha}(1-x)_{g,q}^{\beta}(1+x)_{g,q}^{\gamma} \tag{15}$$

with

$$\begin{aligned}
N_g &= 19.234 - 14.651 \cdot \tilde{s} \\
\alpha_g &= -1.3370 \cdot \tilde{s} \\
\beta_g &= 3.0574 - 2.1984 \cdot \tilde{s} \\
\gamma_g &= -10.836 \cdot \tilde{s} \\
N_q &= 23.026 - 24.217 \cdot \tilde{s} + 16.732 \cdot \tilde{s}^2 \\
\alpha_q &= -1.5052 \cdot \tilde{s} + 1.1115 \cdot \tilde{s}^2 \\
\beta_q &= 2.3813 - 4.8667 \cdot \tilde{s} + 3.9190 \cdot \tilde{s}^2 \\
\gamma_q &= -18.930 \cdot \tilde{s} + 12.265 \cdot \tilde{s}^2
\end{aligned}$$

Here $\tilde{s}$ denotes the scaling variable

$$\tilde{s} = \ln \frac{\ln(\kappa^2/\Lambda^2)}{\ln(\kappa_0^2/\Lambda^2)}$$

with $\kappa_0 = 2$GeV and $\Lambda = 190$MeV. This parametrization is valid in the interval $0.15 \leq x_E \leq 0.75$ in the case of gluon fragmentation function and in the interval $0.15 \leq x_E \leq 0.9$ in the case of quark fragmentation function.

The systematic error of C_A/C_F is obtained from the sources listed in Table 10 which were also discussed in Section 4.1. To obtain systematic errors interpretable like statistical errors, half the difference in the value obtained for C_A/C_F when a parameter is modified from its central value is quoted as the systematic uncertainty. The single errors are added quadratically.

From the fit of the fragmentation functions in dependence of κ_H obtained with the Durham jet finder the colour factor ratio C_A/C_F was determined to be:

$$\frac{C_A}{C_F} = 2.23 \pm 0.09_{stat.} \pm 0.06_{sys.} \tag{16}$$

in good agreement with the expectation of $C_A/C_F = 2.25$. The fitted value of the QCD scale parameter in leading order is $\Lambda_{\mathrm{QCD}} = (397 \pm 113)$ MeV , with a $\chi^2/n.d.f. \sim 1.4$ for 134 degrees of freedom.

Source of systematic error	rel. Error
Minimum number of tracks per jet	0.5%
Minimum angle between the jets and the beam	0.7%
c depleted event sample	0.5%
Variation of the parton jets assignment	2.4%
Sum	2.6%

Table 10: Source of systematic errors in C_A/C_F.

The behaviour of the data for values of $x_E \gtrsim 0.1$ is well represented by the DGLAP evolution. The good agreement fortifies the scaling violation interpretation. The scale E_{jet} again is disfavoured because the fit in this case yields a rather unphysical result for Λ_{QCD} ($\Lambda_{QCD} \geq 2$ GeV). The scale κ_T is disfavoured because of a worse $\chi^2/n.d.f.$ of about 2. Another possible choice of scales, namely a combination of the hardness κ_H for the quark jets and the scale p_1^T of the gluon jets, as predicted by Equation 1, yields:

$$\frac{C_A}{C_F} = 2.14 \pm 0.09_{stat.} \tag{17}$$

in agreement with the result above. Here for the p_1^T scale a range 6 GeV $\leq \mathrm{p_1^T} \leq$ 27.5 GeV was used. The fitted value of Λ_{QCD} is (404 ± 114) MeV, with a $\chi^2/n.d.f \sim 1.4$.

The corresponding results using the Cambridge cluster algorithm are:

$$\frac{C_A}{C_F} = 2.44 \pm 0.12_{stat.}, \qquad \Lambda_{\mathrm{QCD}} = (280 \pm 102)\ \mathrm{MeV}, \tag{18}$$

$$\frac{C_A}{C_F} = 2.35 \pm 0.12_{stat.}, \qquad \Lambda_{\mathrm{QCD}} = (292 \pm 104)\ \mathrm{MeV}\,, \tag{19}$$

for the scale κ_H and the mixed scale respectively, with a comparable $\chi^2/n.d.f$ of ~ 1.4. The systematic uncertainties are similar to those in (16).

The statistically weighted average of the results (16-19) is taken as the central result:

$$\frac{C_A}{C_F} = 2.26 \pm 0.09_{stat.} \pm 0.06_{sys.} \pm 0.12_{clus.,scale}\,. \tag{20}$$

The statistical and the experimental systematic error is taken to be the minimum of the above values assuming the results to be completely correlated. To account for the uncertainty due to the cluster algorithm and the choice of scale the R.M.S. deviation of the four individual results from the central value is given as additional error.

In Figure 17, the slopes as obtained from the fits (Equation 14) to quark and gluon jets for the scale κ_H are plotted as a function of x_E. The typical scaling violation pattern is directly evident. The data are very well represented by the DGLAP expectation for quarks and for gluons (see lines in Figure 17). Furthermore the slopes of the quark fragmentation functions are in a very good agreement with low energy data from TASSO [1]. The stronger scaling violation for gluons compared to quarks is due to the higher colour charge of the gluons. For gluons also the variation of the fitted C_A within the errors is shown as a grey area, indicating that this measurement has a high sensitivity to the colour factor C_A.

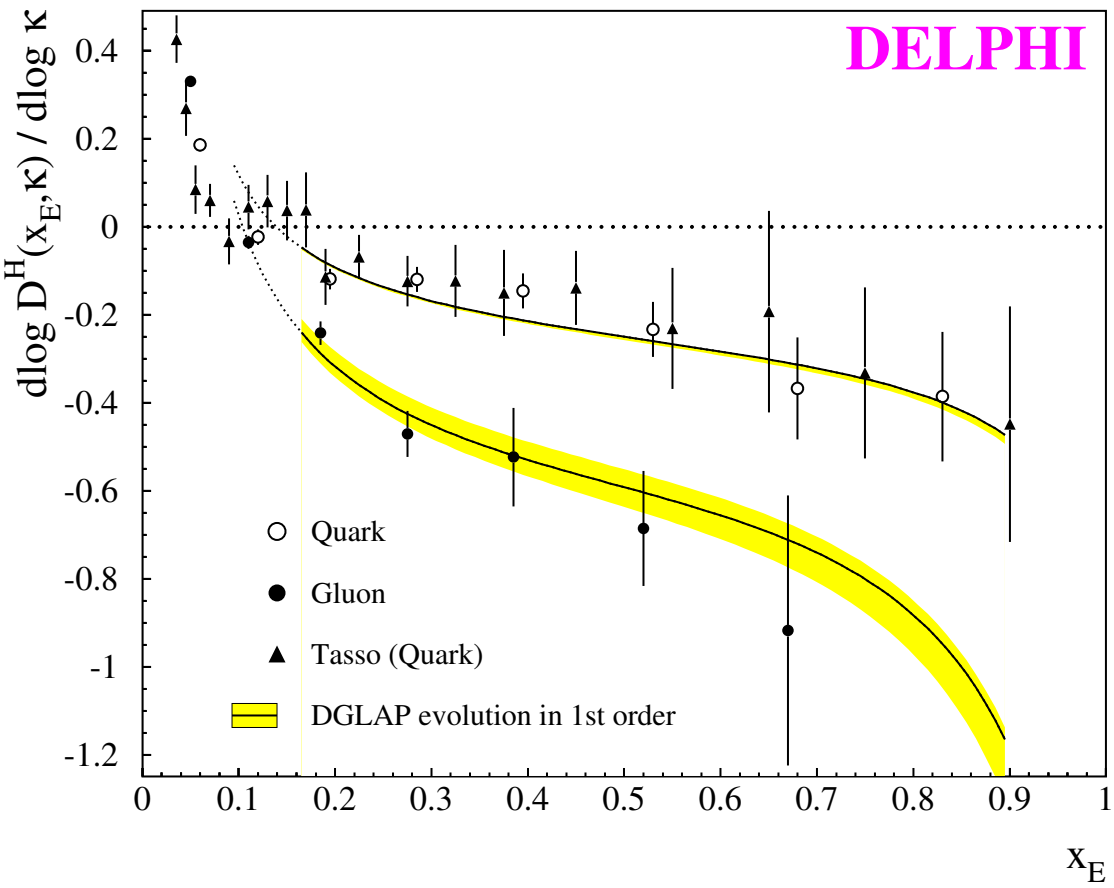

Figure 17: Comparison of scaling violation of quark and gluon jets (Durham algorithm). The full curves show the result from the fit of the DGLAP evolution. The dotted part of the curve is the extrapolation outside the fit range. The grey areas are obtained by changing C_A in the range of the fit errors.

5 Conclusions

Light quark jets and gluon jets of similar transverse momentum-like scales were selected from planar symmetric three-jet events measured with DELPHI. Using impact parameter techniques, gluon jets were selected in heavy quark events. Light quark jets were obtained from heavy quark depleted events. Properties of pure quark and gluon jets were obtained by subtraction techniques.

A measurement of the quark and gluon fragmentation function into stable charged hadrons is presented as a function of the jet scales κ_H and p_1^T. The energy dependence of the ξ distributions illustrates the connection of the increase of the hadron multiplicity with scale and the scaling violation of the fragmentation functions. A good agreement between the measured quark jet fragmentation functions and those obtained from lower (and higher) energy data is observed indicating the proper choice of scales. This choice is confirmed by the study of the jet broadening $< \beta >$ as a function of these scales.

Scaling violations are clearly observed for quark jets as well as for gluon jets. The latter presents evidence for the triple gluon coupling, a basic ingredient of QCD. Scaling violations are observed to be much stronger for gluon compared to quark jets. The colour

factor ratio:

$$\frac{C_A}{C_F} = 2.26 \pm 0.09_{stat.} \pm 0.06_{sys.} \pm 0.12_{clus.,scale}$$

is obtained from the scaling violations in gluon to quark jets by simultaneously fitting the quark and gluon fragmentation functions with a first order QCD DGLAP evolution. This result is equivalent to the most precise measurements of this ratio from the multiplicities in quark and gluon jets [17] and from four-jet angular distributions [33]. A parameterization for the quark and gluon fragmentation functions is given at a reference scale of $\kappa_H = 5.5$ GeV and for a broad range of κ_H.

Acknowledgements

We thank Yu.L. Dokshitzer, V. Khoze, P. Kroll and B.R. Webber for useful and illuminating discussions. We are greatly indebted to our technical collaborators, to the members of the CERN-SL Division for the excellent performance of the LEP collider, and to the funding agencies for their support in building and operating the DELPHI detector.
We acknowledge in particular the support of
Austrian Federal Ministry of Science and Traffics, GZ 616.364/2-III/2a/98,
FNRS–FWO, Belgium,
FINEP, CNPq, CAPES, FUJB and FAPERJ, Brazil,
Czech Ministry of Industry and Trade, GA CR 202/96/0450 and GA AVCR A1010521,
Danish Natural Research Council,
Commission of the European Communities (DG XII),
Direction des Sciences de la Matière, CEA, France,
Bundesministerium für Bildung, Wissenschaft, Forschung und Technologie, Germany,
General Secretariat for Research and Technology, Greece,
National Science Foundation (NWO) and Foundation for Research on Matter (FOM), The Netherlands,
Norwegian Research Council,
State Committee for Scientific Research, Poland, 2P03B06015, 2P03B1116 and SPUB/P03/178/98,
JNICT–Junta Nacional de Investigação Científica e Tecnológica, Portugal,
Vedecka grantova agentura MS SR, Slovakia, Nr. 95/5195/134,
Ministry of Science and Technology of the Republic of Slovenia,
CICYT, Spain, AEN96–1661 and AEN96-1681,
The Swedish Natural Science Research Council,
Particle Physics and Astronomy Research Council, UK,
Department of Energy, USA, DE–FG02–94ER40817.

References

[1] For compilations of a multitude or results on quark fragmentation functions from e^+e^--annihilation and lepton scattering see [27]. Data from the following publications are used in this paper:
TASSO Collaboration, Z. Phys. **C47** (1990) 187;
TPC Collaboration, Phys. Rev. Lett. **61** (1988) 1263;
DELPHI Collaboration, P. Abreu et al., Z. Phys. **C73** (1996) 11;
DELPHI Collaboration, P. Abreu et al., Z. Phys. **C73** (1997) 229;
DELPHI Collaboration, P. Abreu et al., Phys. Lett. **B459** (1999) 397.

[2] V. A. Khoze and W. Ochs, Int. J. Mod. Phys. A **12**, 2949 (1997).

[3] Yu.L. Dokshitzer, V.A. Khoze, A.H. Mueller and S.I. Troyan, *Basics of perturbative QCD*, Editions Frontieres, 1991.

[4] V.N. Gribov and L.N. Lipatov, Sov. J. Nucl. Phys. 15 (1972) 438 and 675;
G. Altarelli and G. Parisi, Nucl. Phys. **B126** (1977) 298;
Yu.L. Dokshitzer, Sov. Phys. JETP **46** (1977) 641.

[5] Yu.L. Dokshitzer and S.I. Troyan in Proc. XIX Winter school of the LNPI 1 p.144;
Yu.L. Dokshitzer and S.I. Troyan, LNPI-922, 1984;
G. Marchesini and B.R. Webber, Nucl. Phys. **B238** (1984) 1;
B.R. Webber, Nucl. Phys. **B238** (1984) 492.

[6] Yu.L. Dokshitzer, private communication. See also [3] and
Yu.L. Dokshitzer, D.I. Dyakonov and S.I. Troyan, Phys. Rep. **58** No. 5 (1980) 269.

[7] DELPHI Collaboration, P. Abreu et al., Z. Phys. **C70** (1996) 179.

[8] OPAL Collaboration, G. Abbiendi et al., CERN-EP/99-028.

[9] R.K. Ellis, W.J. Stirling and B.R. Webber, *QCD and Collider Physics*, Cambridge University Press.

[10] P. Nason and B.R. Webber, Nucl. Phys. **B421** (1994) 473.

[11] The program *evolve* from B. Webber is used.

[12] DELPHI Collaboration, P. Abreu et al., Phys. Lett. **B398** (1997) 194.

[13] ALEPH Collaboration, D. Buskulic et al., Phys. Lett. **B357** (1995) 487 and
Phys. Lett. **B364** (1995) 247 (erratum).

[14] DELPHI Collaboration, P. Aarnio et al., Nucl. Instr. and Methods in Physics Research **A303** (1991) 233.

[15] DELPHI Collaboration, P. Abreu et al., Nucl. Inst. and Meth. **A378** (1996) 57.

[16] S. Catani, Yu.L. Dokshitzer, M. Olsson, G. Turnrock and B.R. Webber, Phys. Lett. **B269** (1991) 432;
S. Bethke, Z. Kunszt, D.E. Soper and W.J. Stirling, Nucl. Phys. **B370** (1992) 310.

[17] DELPHI Collaboration, P. Abreu et al., Phys. Lett. **B449** (1999) 383.

[18] P. Eden and G. Gustafson, JHEP**09**, (1998) 15.

[19] Yu.L. Dokshitzer, G. Leder, S. Moretti and B. Webber, JHEP**08**, (1997) 1;
S. Bentvelsen and I. Meyer, Eur. Phys. J. **C4** (1998) 623.

[20] DELPHI Collaboration, P. Abreu et al., CERN-EP/98–180, accepted by E. Phys. J. C.

[21] T. Sjöstrand, Comp. Phys. Comm. **39** (1986) 346;
T. Sjöstrand and M. Bengtsson, Comp. Phys. Comm. **43** (1987) 367;
T. Sjöstrand, *JETSET 7.3 Program and Manual*, CERN-TH 6488/92.

[22] DELPHI Collaboration, P. Abreu et al., Z. Phys. **C73** (1996) 11.

[23] DELPHI Collaboration, *DELPHI event generation and detector simulation*,
DELPHI 89-67 PROG-142.

[24] ALEPH Collaboration, D. Buskulic et al., Phys. Lett. **B384** (1996) 353.
[25] DELPHI Collaboration, P. Abreu et al., Eur. Phys. J. **C4** (1998) 1.
[26] OPAL Collaboration, R. Akers et al., Z. Phys. **C68** (1995) 179.
[27] HEPDATA database, *http://cpt1.dur.ac.uk/HEPDATA*; see also M. R. Whalley, *HEPDATA - World Wide Web User Guide*, DPDG/96/01.
[28] C.P. Fong and B.R. Webber, Phys. Lett. **B229** (1989) 289.
[29] S. Catani, G. Turnock and B.R. Webber, Phys. Lett. **B295** (1992) 269;
Yu.L. Dokshitzer et al., JHEP**08** (1998) 1.
[30] DELPHI Collaboration, Delphi 99-19 CONF 219 (submitted to XXXIVth Rencontre de Moriond QCD 1999).
[31] O. Klapp, talk given at American Physical Society (APS) Meeting of the Division of Particles and Fields (DPF 99), Los Angeles, USA (5-9 Jan 1999);
Proceedings DPF'99, *Comparing Gluon to Quark Jets with Delphi*, hep-ph/9903398.
[32] J. Binnewies, B.A. Kniehl and G. Kramer, Z. Phys. **C65** (1995) 471.
[33] ALEPH Collaboration, R. Barate et al., Z. Phys. **C76** (1997) 1;
DELPHI Collaboration, P. Abreu et al., Phys. Lett. **B414** (1997) 401;
OPAL Collaboration, R. Akers et al., Z. Phys. **C68** (1995) 519.